Global Omori law decay of triggered earthquakes: Large aftershocks outside the classical aftershock zone

Tom Parsons

U.S. Geological Survey, Menlo Park, California, USA

[1]   Triggered earthquakes can be large, damaging, and lethal as evidenced by the1999 shocks in Turkey and the 2001 earthquakes in El Salvador. In this study, earthquakes with $M_s \geq 7.0$ from the Harvard centroid moment tensor (CMT) catalog are modeled as dislocations to calculate shear stress changes on subsequent earthquake rupture planes near enough to be affected. About 61% of earthquakes that occurred near (defined as having shear stress change $|\Delta\tau| \geq 0.01$ MPa) the $M_s \geq 7.0$ shocks are associated with calculated shear stress increases, while ~39% are associated with shear stress decreases. If earthquakes associated with calculated shear stress increases are interpreted as triggered, then such events make up at least 8% of the CMT catalog. Globally, these triggered earthquakes obey an Omori law rate decay that lasts between ~7–11 years after the main shock. Earthquakes associated with calculated shear stress increases occur at higher rates than background up to 240 km away from the main shock centroid. Omori's law is one of the few time-predictable patterns evident in the global occurrence of earthquakes. If large triggered earthquakes habitually obey Omori's law, then their hazard can be more readily assessed. The characteristic rate change with time and spatial distribution can be used to rapidly assess the likelihood of triggered earthquakes following events of $M_s \geq 7.0$. I show an example application to the $M = 7.7$ 13 January 2001 El Salvador earthquake where use of global statistics appears to provide a better rapid hazard estimate than Coulomb stress change calculations.   *INDEX TERMS:* 7223 Seismology: Seismic hazard assessment and prediction; 7230 Seismology: Seismicity and seismotectonics; 8164 Tectonophysics: Evolution of the Earth: Stresses—crust and lithosphere; 7209 Seismology: Earthquake dynamics and mechanics; *KEYWORDS:* earthquake triggering, aftershocks, Omori's law, seismicity rate, seismicity distribution, earthquake probability

1. Introduction

[2] Aftershocks are defined as events of lesser magnitude following a larger main shock that are distributed over the fracture area of the main shock [e.g., *Uidas*, 1999]. In 1894, Omori noted that the rate of aftershocks decays with time approximately as t^{-1} following the main shock; a slightly better fit can be made by applying $c/(p + t)^n$ [*Utsu*, 1961], where c, p, and n are constants that vary with each sequence, with n usually about equal to one. Triggered earthquakes occur where the stress redistribution caused by the main shock encourages earthquakes away from the main shock rupture plane. The exponential decay in the rate of aftershocks is one of the few reliably time-predictable patterns of earthquake occurrence. In this paper I show that large, triggered earthquakes have the same time-predictable occurrence as aftershocks.

[3] Aftershocks occurring on or near the rupture plane are thought to be a result of incomplete rupture and/or hetero-geneous slip [e.g., *Bullen and Bolt*, 1947]. The disruption caused by the main shock has also been invoked to explain aftershocks away from the primary rupture plane; for example, *Dutton* [1904, p. 62] states "…portions of the raised or sunken mass are subject to stresses which from time to time give rise to further movements. . . ." *Dutton*'s [1904] explanation is validated by calculations of static stress changes following large earthquakes that correlate with the pattern of off-fault aftershocks [*Harris*, 1998, and references therein]. Static stress change calculations have also provided an explanation for seismicity rate increases and decreases that occur well outside the above defined aftershock zone [e.g., *King et al.*, 1994; *Reasenberg and Simpson*, 1992].

[4] Limited study of the rate of triggered earthquakes outside the classical aftershock zone shows clusters that exhibit the same temporal decay as aftershocks, implying that the process of stress transfer may apply to all the events. I note some examples below, which motivate the questions, how general is this occurrence? How far from the main shock does it occur? What size earthquakes are observed in these exponentially decaying sequences? And, can this information be applied to hazard assessment?
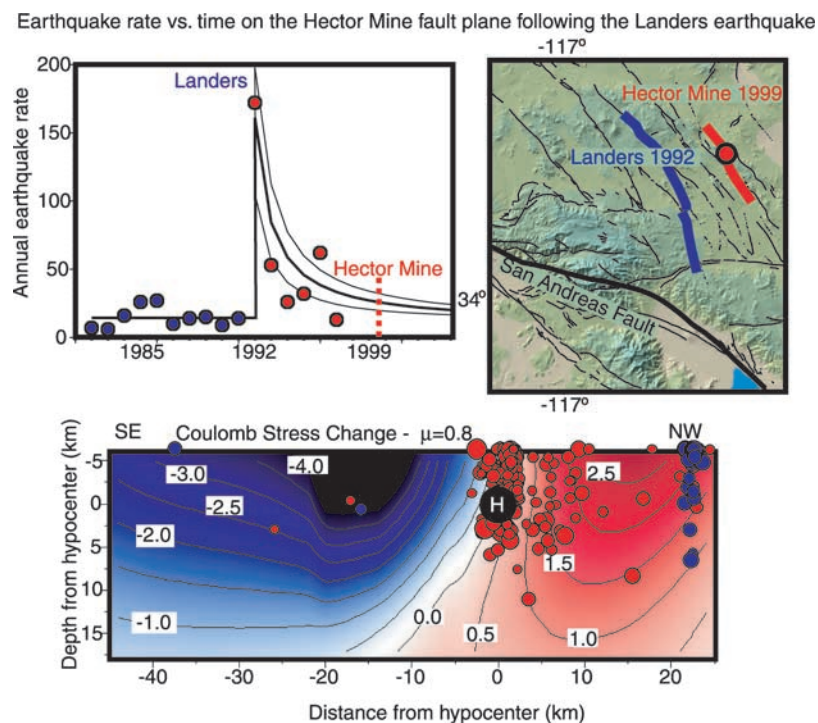
Earthquake rate vs. time on the Hector Mine fault plane following the Landers earthquake

Figure 1. The annual rate of earthquakes following the 1992 $M = 7.4$ Landers earthquake near the eventual hypocenter of the 1999 $M = 7.1$ Hector Mine earthquake follows an exponential decay with time. The decay rate was fit roughly to a t^{-1} curve. Coulomb stress change from the Landers earthquake [*Parsons and Dreger*, 2000] is shown calculated on the Hector Mine rupture plane of *Dreger and Kaverina* [2000] (corresponds to the red line on the location map). Earthquake hypocenters [*Richards-Dinger and Shearer*, 2000] located within 1 km of the Hector Mine rupture plane are shown for the periods of 5 years before (blue) and after (red) the Landers earthquake. The rate plot was made with the same events using 1-year bins. The Hector Mine earthquake occurred when the seismicity rate was slightly above background. Thus the Hector Mine earthquake could be considered another, albeit large, aftershock of the Landers main shock.

1.1. Landers-Hector Mine Earthquakes

[5] The 16 October 1999 $M = 7.1$ Hector Mine earthquake occurred ~30 km northeast of the 1992 $M = 7.3$ Landers earthquake in southern California (Figure 1). After the Landers earthquake, a swarm of mostly small earthquakes began occurring on a completely different fault near the eventual hypocenter of the Hector Mine earthquake, and correlated spatially with an area where Coulomb stress increases were calculated [*Parsons and Dreger*, 2000]. The Hector Mine hypocenter occurred where neutral or undetermined Coulomb stress change was calculated [*Harris and Simpson*, 2002], though most Hector-Mine slip happened where Coulomb stress was calculated to have been increased by the Landers shock [*Parsons and Dreger*, 2000; *Pollitz*, 2002]. The Coulomb failure criterion (ΔCF) is defined by $\Delta CF \equiv |\Delta\bar{\tau}_f| + \mu(\Delta\sigma_n + \Delta p)$, where $\Delta\bar{\tau}_f$ is the change in shear stress on the receiver fault, μ is the coefficient of friction, $\Delta\sigma_n$ is the change in normal stress acting on the receiver fault, and Δp is pore pressure change.

[6] The swarm of post-Landers earthquakes occurring on the Hector Mine fault plane (located within ±1 km of the rupture plane) shows a rough Omori law decay in the rate of earthquakes with time until the occurrence of the Hector Mine event (Figure 1), which was followed by its own set of

aftershocks. The Hector Mine earthquake could thus be interpreted as a Landers aftershock. If that view is correct, then the $M = 7.1$ Hector Mine earthquake was expected, albeit at low probability, within the bounds of the Omori rate decay, and within the regions of heightened stress change.

1.2. Loma Prieta

[7] The 19 October 1989 $M = 7.1$ Loma Prieta earthquake affected San Francisco Bay area faults within a ~50 km radius from the epicenter in the Santa Cruz Mountains [*Reasenberg and Simpson*, 1992; *Parsons et al.*, 1999]. The complex rupture caused both Coulomb stress increases and decreases on subparallel faults; in Figure 2, an example is shown where stress was increased on the offshore San Gregorio fault and another where stress was decreased on the south Hayward fault east of San Francisco Bay. The annual rate of microseismicity (earthquakes occurring within ±1 km of the receiver fault plane) immediately increased on the San Gregorio fault following the Loma Prieta earthquake and has been subsiding exponentially with time, following an Omori law rate decay (Figure 2). The opposite case is observed on the south Hayward fault where the annual microseismicity rate declined sharply after the stress decrease from the Loma Prieta shock and has gradually returned to
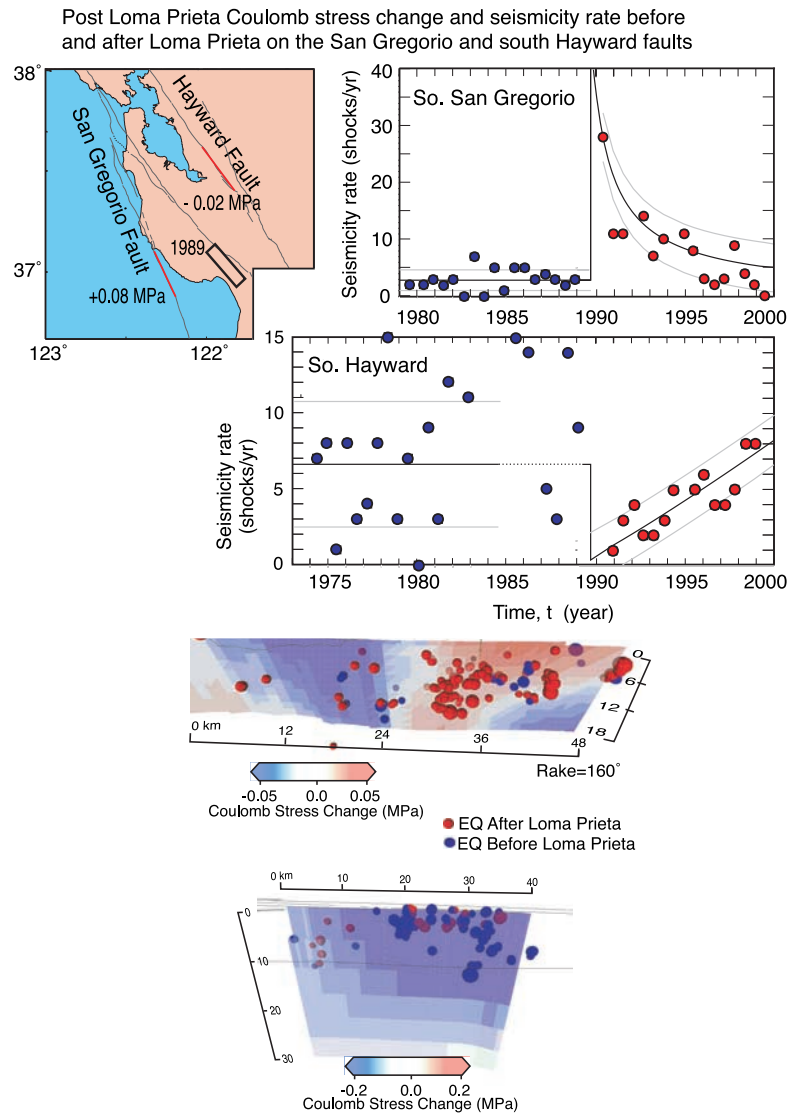
Figure 2. Microseismicity rates on the San Gregorio and Hayward faults were affected by the 1989 $M = 7.1$ Loma Prieta earthquake. Coulomb stress changes and earthquake hypocenters are shown projected onto the San Gregorio fault (above) and south Hayward fault (below) [*Parsons et al.*, 1999]; cross sections correspond to the red lines on the location map and are shown from north at the left to south. Where Coulomb stress was calculated to have been increased on the San Gregorio fault, seismicity began occurring at sharply higher rates, then declined on a t^{-1} trend. Where Coulomb stress was decreased on the south Hayward fault, seismicity rates dropped, then recovered on an inverse Omori law trend, linear with t. Seismicity rate plots were made using the hypocenters selected within ±1 km of the fault planes, as shown on the stress change plots, with 1-year bins.

background rates following an inverse Omori law trend (linear with time; Figure 2).

1.3. North Anatolian Fault

[8] The 17 August 1999 $M = 7.4$ Izmit earthquake was closely followed by the 12 November 1999 $M = 7.1$ Düzce earthquake. Combined, these two earthquakes killed at least 18,000 people, destroyed 15,400 buildings, and caused $10-25$ billion in damage. The Izmit earthquake occurred where the Coulomb failure stress was calculated to have increased $0.1-0.2$ MPa by $M \geq 6.8$ earthquakes since 1939 (Figure 3) [*Stein et al.*, 1997]. The Izmit event, in turn, increased stress beyond the east end of the rupture by $0.1-$ 0.2 MPa, where the $M = 7.1$ Düzce earthquake struck, and by $0.05-0.5$ MPa beyond the west end of the 17 August rupture, where a cluster of aftershocks occurred [*Parsons et al.*, 2000].

[9] Stress triggering was invoked to explain the 60-year sequence of earthquakes rupturing toward Istanbul along the North Anatolian fault, in which all but one event promoted the next [*Stein et al.*, 1997]. The thirteen $M \geq 6.8$ North Anatolian earthquakes for which the stress at the future epicenter was increased by ≥ 0.05 MPa were stacked in time bins as a function of the delay between the triggering and subsequent earthquakes [*Parsons et al.*, 2000] (Figure 3). The time bins show the annual rate of $M \geq 6.8$ earthquakes
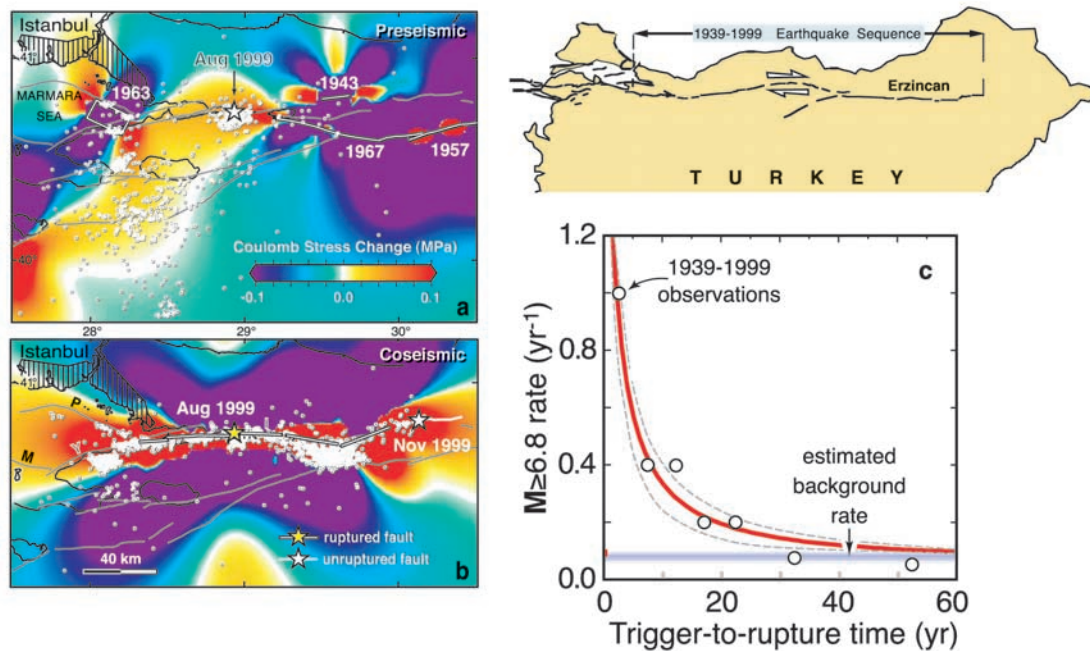
Figure 3. On the North Anatolian fault zone of western Turkey, the 17 August 1999 M = 7.4 Izmit earthquake was the most westerly in a series of progressing earthquakes where Coulomb stress at each rupture was increased by the preceding earthquakes [e.g., *Stein et al.*, 1997]. The 12 November 1999 M = 7.1 Düzce earthquake occurred in a heightened stress region from the Izmit shock. The delays between triggering and triggered earthquakes in the sequence from 1939 to 1999 are plotted as a histogram with each white dot corresponding to a time bin [*Parsons et al.*, 2000]. The plot shows how many triggered earthquake pairs fall within each time delay window. The majority of earthquakes are triggered rapidly, with the rate falling off as a function of time as t^{-1} just like aftershocks.

along the North Anatolian fault, which decays as t^{-1} in a manner identical to aftershocks (Figure 3). Some of the triggering events in the North Anatolian sequence might be considered foreshocks in that they were smaller than the triggered earthquakes that followed them.

[10] The above three examples provide the motivation for this study. There is a tendency for Omori law decay in the rate of triggered earthquakes as time passes that, in the three cases investigated, is independent of earthquake size, occurs well outside the classically defined aftershock zone, and can include what might be considered foreshocks (triggering earthquake smaller than triggered). Because Omori's law is perhaps the only globally reliable, time-predictable pattern of earthquake occurrence and because the examples given above show that some of the earthquakes falling within that pattern can be large and deadly, I investigate here the global occurrence of triggered earthquakes in the Harvard centroid moment tensor (CMT) catalog [e.g., *Dziewonski et al.*, 1981], and their rate as a function of time.

2. Triggered Earthquakes in the Harvard CMT Catalog

2.1. Methods

[11] In this paper, examples of triggered earthquakes behaving like aftershocks have been given for three regional earthquake sequences. To make a more general study on the temporal behavior of triggered earthquakes, I use the Harvard CMT catalog [e.g., *Dziewonski et al.*, 1981].

CMT solutions are produced on a routine basis for events with surface wave magnitudes (M_s) greater than ∼5.5. The catalog covers the time span from January 1977 until September 2000 and includes 17,402 earthquakes, some of which have magnitudes down to the M_s 4.5 level. I selected from the CMT catalog all $M_s \geq 7.0$ earthquakes as candidates for inducing triggering; the choice of $M_s \geq 7.0$ earthquakes to act as triggers was made in advance and was not changed during the course of the study. From this group I removed any earthquakes that occurred within one degree of a previous $M_s \geq 7.0$ shock as potentially triggered, even if it was larger than its predecessor. I then selected all events that have been studied sufficiently well so that the correct nodal plane could be chosen, or that occurred in tectonic settings where a nodal plane could be assigned with reasonable confidence (for example, along a major strike-slip fault zone or located on the interplate contact of a subduction zone). This selection process resulted in 117 $M_s \geq 7.0$ earthquakes of known mechanism that may have caused sufficient static stress change to trigger earthquakes (Table 1) (Figure 4).

[12] All stress change calculations were resolved on dislocation planes; no point calculations were used. The strike, dip, and rake (mostly from CMT solutions) of the 117 $M_s \geq 7.0$ earthquakes were used to create the elastic dislocation models. Dislocation length, width, and slip were determined from the global regressions of *Wells and Coppersmith* [1994]. Using the centroid locations of the 117 $M_s \geq 7.0$ earthquakes, the CMT catalog was searched for all

**Table 1.** The 117 $M_s \geq 7.0$ Earthquakes Used in This Study[a]

Earthquake	Date	M_s	Latitude	Longitude	Depth, km	Strike, deg	Dip, deg	Rake, deg	Number of Earthquakes Increase	Number of Earthquakes Decrease	Nodal Plane Ref.
Luzon	1977	7.0	16.380	122.590	35.0	207	27	108	1	1	1
Solomon Islands	1977	7.2	−8.160	155.920	24.3	272	80	34	6	11	1
Sumba	1977	7.9	−11.140	118.230	23.3	270	45	−70	31	18	2
South of Tonga Islands	1977	7.4	−26.100	−31.220	23.4	180	55	−95	2	2	3
San Juan Province, Argentina	1977	7.4	−31.220	−67.690	20.8	10	45	80	6	5	4
Kermadec Islands	1978	7.2	−30.600	−177.020	23.1	26	61	95	18	4	1
Kuril Islands	1978	7.5	44.120	149.270	28.3	224	11	91	69	13	5
East Coast of Honshu Japan	1978	7.7	38.020	142.070	37.7	184	14	59	38	13	1
Taiwan Region	1978	7.4	22.010	121.600	28.9	5	61	69	0	3	6
Oaxaca, Mexico	1978	7.7	16.220	−96.560	16.1	270	14	54	18	9	7
Tabas, Iran	1978	7.4	33.390	57.430	33.0	328	33	107	2	1	8
St. Elias, Alaska	1979	7.3	60.500	−141.390	18.8	320	26	149	2	1	9
Petatlan (near Guerrero, Mexico)	1979	7.6	17.780	−101.370	26.7	293	14	110	13	10	10
Yapen (Irian Java)	1979	7.9	−1.780	136.060	16.3	100	71	5	24	42	11
Puysegur Bank (New Zealand)	1979	7.4	−46.540	165.770	20.3	339	78	90	1	0	12
Tumaco, Colombia	1979	7.7	2.320	−78.810	24.0	121	20	90	12	10	13
Kuril Islands 1980	1980	7.0	43.210	146.910	33.6	213	15	89	16	22	5
Santa Cruz Islands	1980	7.5	−12.920	166.210	43.6	157	42	78	3	0	14
Algeria, El Asnam	1980	7.3	36.250	1.360	10.1	50	61	81	4	5	15
Loyalty Islands	1980	7.2	−21.760	169.840	28.8	330	23	103	37	15	16
Eureka, California	1980	7.2	41.140	−124.360	15.0	51	89	27	2	10	17
Rat Islands	1981	7.0	51.520	176.100	20.0	275	22	114	4	3	18
New Zealand, Macquarie Ridge	1981	7.6	−48.940	164.390	33.3	33	85	−173	4	2	19
Vanuatu Islands	1981	7.1	−17.340	167.270	30.0	338	27	83	8	12	20
Iran	1981	7.1	30.030	57.580	15.2	250	13	119	2	1	21
Samoa Islands	1981	7.7	−15.020	−173.160	20.0	273	55	−103	71	52	22
Michoacan (Playa Azul)	1981	7.3	18.280	−102.000	31.8	287	20	82	12	6	23
Guerrero Mexico (Ometepec)	1982	7.0	16.930	−98.320	18.6	121	79	93	8	4	24
Greece	1983	7.0	38.130	20.380	10.1	34	14	153	1	4	25
Costa Rica	1983	7.2	8.850	−83.250	28.0	310	25	110	3	3	26
Honshu, Japan	1983	7.7	40.440	138.870	12.6	16	27	86	5	3	27
Coast of northern Chile	1983	7.3	−26.010	−70.560	38.7	9	20	110	7	7	1
Borah Peak, Idaho	1983	7.3	44.350	−113.980	13.7	138	62	−83	0	3	28
Uzbekistan (Gazli)	1984	7.0	40.590	63.240	15.0	41	69	91	0	1	29
Kuril Islands	1984	7.1	44.170	148.620	30.6	229	17	109	20	10	1,5
Mid-Atlantic Ridge	1984	7.1	8.360	−38.820	10.0	274	73	−177	3	3	1
North Sumatera	1984	7.2	−0.230	97.840	24.7	334	10	116	4	1	1
Kamchatka	1984	7.0	56.240	163.800	21.5	260	61	162	5	2	1
Chile (Valparaiso)	1985	7.8	−33.920	−71.710	40.7	11	26	110	12	1	30
New Britain	1985	7.1	−5.680	150.970	25.4	97	77	−23	0	1	31
New Britain	1985	7.2	−4.280	152.580	31.4	169	37	106	2	1	1
West Irian Jaya	1985	7.1	−1.630	134.710	13.3	271	85	26	4	7	11
Vanuatu (South Solomon trench)	1985	7.0	−14.070	166.090	24.2	4	56	−77	9	11	1
Andreanof Islands	1986	7.7	51.330	−175.430	31.3	246	22	85	50	13	32
Papua New Guinea	1986	7.1	−4.420	143.640	99.7	320	19	114	4	5	1
Kermadec Islands	1986	8.2	−27.930	−176.070	40.0	13	74	45	80	75	33
Taiwan (Lotung/Hualien)	1986	7.8	23.970	121.850	33.2	210	33	87	49	43	34
Papua New Guinea	1987	7.4	−5.900	147.720	15.0	82	83	4	39	35	1
North coast of Chile	1987	7.3	−24.380	−70.930	41.9	12	23	106	10	4	35
New Britain	1987	7.4	−6.220	149.440	47.8	262	32	90	41	10	36
Gulf of Alaska	1987	7.6	58.170	−142.040	15.0	262	82	−20	0	5	37
Coast of Peru	1988	7.0	−17.550	−72.830	15.0	322	11	87	3	2	1
Burma-India border	1988	7.2	25.190	94.890	100.5	284	45	55	6	2	1
Lancang-Gengma, China	1988	7.3	23.000	99.680	15.0	333	78	174	1	7	38
Macquarie Ridge	1989	8.3	−52.150	160.410	15.0	34	69	170	4	6	39
Loma Prieta	1989	7.1	37.060	−121.630	19.0	235	41	123	0	0	40
Solomon Islands	1989	7.1	−10.950	162.300	25.2	272	21	22	15	1	1
Honshu, Japan (Iwaizumi)	1989	7.3	39.950	143.080	24.0	183	14	69	39	10	41
Mindinao Philippines	1989	7.4	7.880	126.960	36.9	176	34	66	30	17	1
Fiji basin	1990	7.5	−22.050	175.350	25.3	228	68	4	5	5	1
Costa Rica	1990	7.0	9.950	−84.580	17.9	303	11	104	4	1	42
Mariana Islands	1990	7.5	15.570	148.080	15.0	185	31	−108	3	9	43
Minahasa Peninsula	1990	7.4	1.310	123.350	33.2	112	31	122	27	16	44
Sudan	1990	7.2	5.320	32.290	15.0	315	86	23	4	2	45
Iran	1990	7.7	36.950	49.520	15.0	300	73	32	2	2	46
Luzon Philippines	1990	7.7	15.970	121.230	10.0	153	89	16	10	17	47
Komandorsky Islands	1990	7.0	53.770	169.410	26.6	308	23	159	1	0	48
Valle de la Estrella, Costa Rica	1991	7.5	10.100	−82.770	15.0	103	25	58	6	1	49
Racha-Dzhava Caucasus	1991	7.0	42.600	43.610	22.3	288	39	106	1	1	50

Table 1. (continued)

Earthquake	Date	M_s	Latitude	Longitude	Depth, km	Strike, deg	Dip, deg	Rake, deg	Number of Earthquakes Increase	Number of Earthquakes Decrease	Nodal Plane Ref.
Uttarkashi, Himalaya	1991	7.1	30.22	78.24	15	317	14	115	0	0	51
Columbia	1991	7.0	4.800	−77.180	19.1	13	13	95	0	1	1
Kuril Islands	1991	7.4	45.580	151.550	31.2	226	16	99	21	7	1
Cape Mendocino	1992	7.1	40.250	−124.310	15.0	331	9	68	4	0	52
Landers	1992	7.5	34.650	−116.650	15.0	341	70	−172	4	3	53
Susamyr (Kyrgyzstan)	1992	7.4	42.190	73.320	17.0	88	60	99	1	0	54
Ascension Island	1992	7.0	−0.710	−13.540	15.0	256	81	−179	2	1	1
Nicaragua	1992	7.2	11.200	−87.810	15.0	303	12	91	12	1	46
Colombia	1992	7.3	7.270	−76.340	15.0	9	81	46	1	4	55
Flores Indonesia	1992	7.5	−8.340	122.490	20.4	80	40	95	6	2	56
Hokkaido (Kushiro-Oki)	1993	7.1	43.060	144.290	100.0	133	6	−36	3	1	57
Kamchatka	1993	7.3	51.360	158.750	45.9	207	29	79	7	0	58
Guam	1993	8.1	13.060	145.310	59.3	312	18	147	29	14	59
Ormond (Fiordland) New Zealand	1993	7.1	−45.040	166.730	15.0	46	29	127	1	0	60
Chiapas-Guatemala	1993	7.3	14.410	-92.990	29.1	289	24	76	16	8	1
Halmahera Indonesia	1994	7.2	1.200	127.800	15.0	351	84	−24	2	4	1
Vanuatu Islands	1994	7.2	−20.450	169.040	42.5	335	40	90	11	5	61
Liwa, Indonesia	1994	7.0	−5.150	104.270	16.2	315	71	176	0	0	62
Java	1994	7.2	−11.030	113.040	15.0	278	7	89	14	1	63
Arthur's Pass New Zealand	1994	7.1	−42.940	171.470	15.0	68	63	150	3	0	64
Kuril Islands	1994	8.1	43.710	147.330	33.0	50	74	128	38	51	65
Mindoro, Philippines	1994	7.1	13.440	121.320	15.0	339	70	−178	2	1	63
Sanriku, Japan	1994	7.5	40.560	142.990	27.7	179	12	67	39	3	66
Kobe	1995	6.8	34.780	134.990	20.3	230	79	160	0	0	67
Tonga	1995	8.0	−15.370	−173.150	87.9	298	84	73	23	17	68
Samar, Phillipines	1995	7.0	12.170	126.030	15.0	145	26	43	12	4	1
Neftegorsk, Sakhalin	1995	7.6	53.030	142.650	23.6	196	82	169	2	3	69
Antofagasta, Chile	1995	7.3	−24.170	−70.740	28.7	354	22	87	4	2	70
Solomon Islands	1995	7.8	−5.510	153.640	45.6	320	48	92	45	32	5
Macas, Ecuador	1995	7.0	−2.550	−77.530	25.0	234	39	120	3	1	71
Colima-Jalisco, Mexico	1995	7.3	19.340	−104.800	15.0	302	9	92	2	0	72
Gulf of Aqaba, Egypt	1995	7.3	29.070	34.730	18.4	196	59	−15	1	2	73
Minahassa, Indonesia	1996	7.7	0.740	119.930	15.0	36	6	54	13	10	1
Biak, Indonesia	1996	8.1	−0.670	136.620	15.0	103	11	69	14	10	11
Aleutian Islands	1996	7.6	51.100	−177.410	29.0	248	17	84	30	6	74
Peru	1996	7.3	−15.040	−75.370	37.4	312	33	55	5	1	75
Quetta, Pakistan	1997	7.3	29.740	68.130	15.3	298	15	122	4	2	76
Iran	1997	7.3	33.580	60.020	15.0	338	90	−173	1	2	77
Tibet	1997	7.9	35.330	86.960	16.4	79	69	2	0	0	78
Kamchatka	1997	7.6	54.310	161.910	33.6	202	23	74	14	2	79
Antarctic plate	1998	8.0	−62.990	148.640	28.8	281	84	17	0	4	80
Offshore SE Taiwan	1998	7.3	22.370	125.530	22.9	49	89	172	1	3	1
Papua New Guinea	1998	7.1	−2.500	142.070	15.0	287	75	78	0	2	81
Coastal Ecuador	1998	7.1	−0.570	−80.480	25.6	27	15	124	2	0	1
Banda Sea (Indonesia)	1998	7.0	−6.940	128.950	24.6	289	37	111	2	1	1
Seram Sea (Indonesia)	1998	7.7	−2.030	125.000	16.4	92	63	−28	8	1	1
Izmit	1999	7.8	41.010	29.970	17.0	91	87	164	2	5	82
Hector Mine	1999	7.4	34.710	−116.270	15.0	336	80	174	0	0	83
Totals									1327	839	

[a] Source parameters from CMT solutions are given along with locations and magnitudes. The number of earthquakes in the CMT catalog associated with calculated shear stress increases and decreases is given for each event. The choice of nodal planes for use in dislocation models was guided by studies of individual earthquakes or local tectonics. The reference codes are as follows: 1, local tectonics; 2, *Lynnes and Lay* [1988]; 3, *Eissler and Kanamori* [1982]; 4, *Langer and Hartzell* [1996]; 5, *Schwartz* [1999]; 6, *Chou and Wang* [1992]; 7, *Chael and Stewart* [1982]; 8, *Hartzell and Mendoza* [1991]; 9, *Estabrook et al.* [1992]; 10, *Mendoza* [1995]; 11, *Okal* [1999]; 12, *Webb and Lowry* [1982]; 13, *Kanamori and McNally* [1982]; 14, *Houston and Kanamori* [1986]; 15, *Bezzeghoud et al.* [1995]; 16, *Vidale and Kanamori* [1983]; 17, *Ellsworth* [1990]; 18, *Ryan and Scholl* [1993]; 19, *Ruff et al.* [1982]; 20, *Chatelain et al.* [1983]; 21, *Berberian et al.* [1984]; 22, *Needham et al.* [1982]; 23, *Mikumo et al.* [1998]; 24, *Astiz and Kanamori* [1984]; 25, *Kiratzi and Langston* [1991]; 26, *Adamek et al.* [1987]; 27, *Satake* [1985]; 28, *Pierce and Morgan* [1992]; 29, *Bossu and Grasso* [1996]; 30, *Mendoza et al.* [1994]; 31, *Mori et al.* [1987]; 32, *Ekstrom and Engdahl* [1989]; 33, *Lundgren et al.* [1989]; 34, *Zheng et al.* [1995]; 35, *Ihmle and Ruegg* [1997]; 36, *Dmowska et al.* [1991]; 37, *Pegler and Das* [1996]; 38, *Mozaffari et al.* [1999]; 39, *Velasco et al.* [1995]; 40, *Wald* [1991]; 41, *Kisslinger and Hasegawa* [1991]; 42, *Protti et al.* [1995]; 43, *Yoshida et al.* [1992]; 44, *Tanioka and Hsu* [1990]; 45, *Girdler and McConnell* [1994]; 46, *Zhang* [1998]; 47, *Velasco et al.* [1996]; 48, *Zobin* [1990]; 49, *Protti and Schwartz* [1994]; 50, *Fuenzalida et al.* [1997]; 51, *Cotton et al.* [1996]; 52, *Hagerty and Schwartz* [1996]; 53, *Wald and Heaton* [1994]; 54, *Mellors et al.* [1997]; 55, *Ammon et al.* [1994]; 56, *Beckers and Lay* [1995]; 57, *Ozel and Moriya* [1999]; 58, *Johnson et al.* [1995]; 59, *Campos et al.* [1996]; 60, *Van Dissen et al.* [1994]; 61, *Calmant et al.* [1997]; 62, *Duquesnoy et al.* [1996]; 63, *Tanioka and Satake* [1996]; 64, *Robinson et al.* [1995]; 65, *Piatanesi et al.* [1999]; 66, *Nakayama and Takeo* [1997]; 67, *Wald* [1996]; 68, *Millen and Hamburger* [1998]; 69, *Rogozhin* [1996]; 70, *Sobiesiak* [2000]; 71, *Yepes* [1996]; 72, *Mendoza and Hartzell* [1999]; 73, *Pinar and Turkelli* [1997]; 74, *Tanioka and Gonzalez* [1998]; 75, *Swenson and Beck* [1999]; 76 *Khan et al.* [1999]; 77 *Balakina et al.* [2000]; 78, *Xu and Chen* [1999]; 79, *Wha* [1998]; 80, *Kreemer and Holt* [2000]; 81, *Kikuchi et al.* [1999]; 82, *Reilinger et al.* [2000]; 83, *Dreger and Kaverina* [2000].

117 Ms>7 earthquakes with identifiable nodal planes considered possible sources of triggering
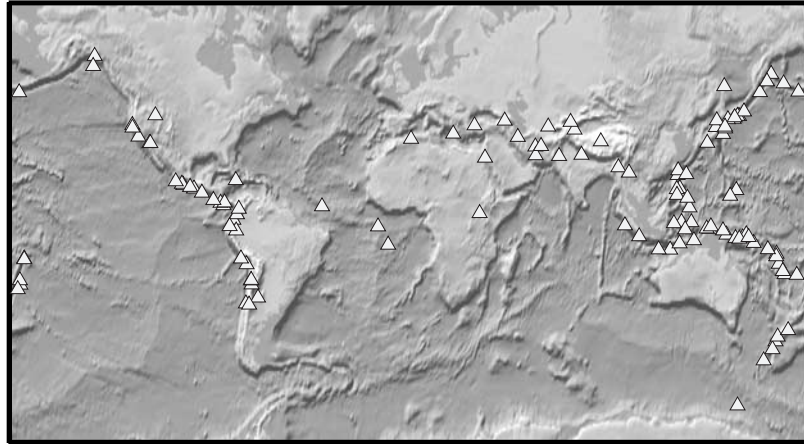
1327 earthquakes within ±2° of triggering events with 0.01-1 MPa shear stress increase
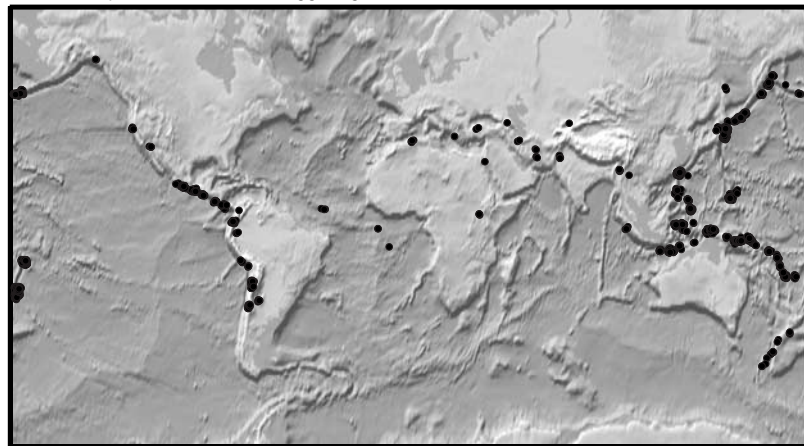
Figure 4. Locations of the 117 $M_s \geq 7.0$ earthquakes modeled as sources of triggering stress (white triangles). Subsequent earthquakes associated with calculated shear stress increases are shown as solid dots.

other earthquakes that occurred within ±2° any time after the $M_s \geq 7.0$ events. Nodal planes of these earthquakes were represented as nonslipping dislocations, or receiver faults. I used the program DLC, written by R. Simpson (based on the subroutines of *Okada* [1992]), to calculate changes in shear stress on receiver fault surfaces caused by slip on source faults in an elastic half-space.

[13] The global nature of this study necessitated calculation of the shear stress component on the receiver faults rather than Coulomb stress change for three reasons: (1) since the shear stress change is equal on both receiver fault nodal planes, it was not necessary to identify the correct one for thousands of earthquakes, (2) Coulomb stress change calculation requires estimation of a friction coefficient for each receiver fault, and (3) Coulomb stress change calculation requires assumptions to be made about coseismic pore fluid pressure changes on each receiver fault. These parameters are estimable in detailed local studies, but cannot be assigned globally with reasonable confidence [e.g., *Beeler et al.*, 2000]. By calculating only the shear stress component I neglect potential triggering and/or inhibition of earthquakes due to normal stress changes, which in

localized studies, have been shown to be important [e.g., *Perfettini et al.*, 1999; *Parsons et al.*, 1999]. However, in other studies using global catalogs, *Kagan* [1994] and *Kagan and Jackson* [1998] find little correlation between normal stress change and earthquake triggering, and they conclude that shear stress changes are most important.

[14] Shear stress changes were calculated, parallel to the CMT solution rake, on nodal planes of all earthquakes that occurred after, and within ±2° of the 117 $M_s \geq 7.0$ source events. These planes were modeled as nonslipping dislocations with length and width determined from the regressions of *Wells and Coppersmith* [1994]. Receiver faults that had calculated shear stress changes between ±0.01 and ±1 MPa were included as potentially influenced by the source earthquakes. The lower threshold for triggering has been shown by previous studies [e.g., *Reasenberg and Simpson*, 1992; *Hardebeck et al.*, 1998; *Harris*, 1998]. The upper threshold was set to prevent calculations on planes very close (∼10 km or closer) to the source plane, which are highly sensitive to the details of the source slip model [e.g., *Simpson and Reasenberg*, 1994]. Selection of potentially triggered earthquakes by magnitude of stress change rather than by a
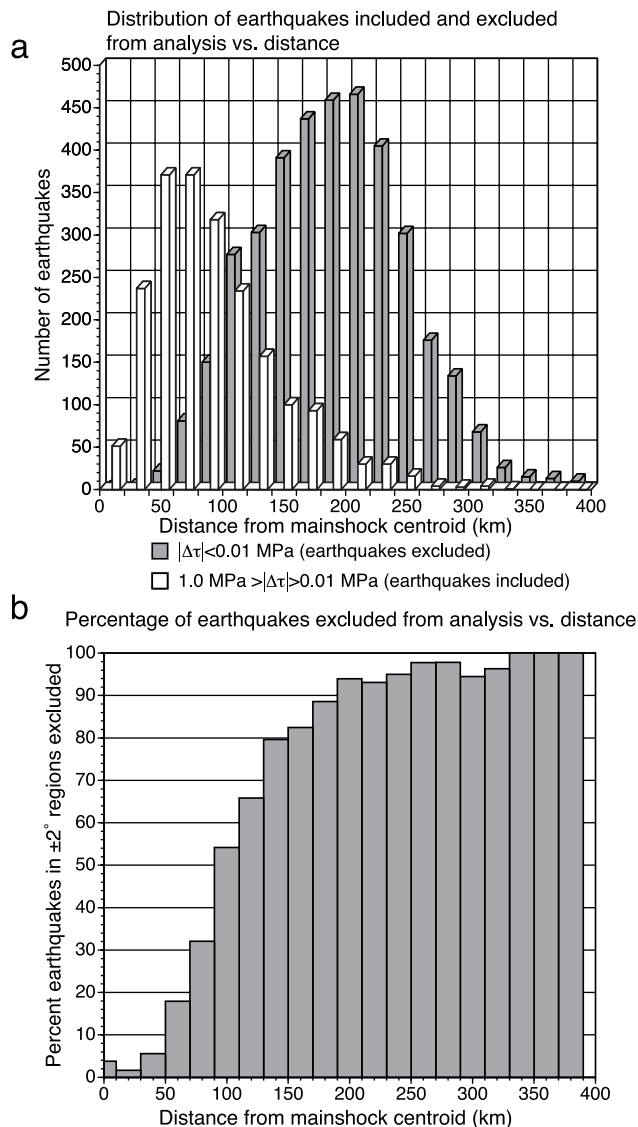
Figure 5. (a) Distribution of earthquakes included (open columns; 0.01 MPa < $|\Delta\tau|$ < 1.0 MPa) and excluded (shaded columns; $|\Delta\tau| \leq 0.01$ MPa) in this study as a function of distance between the main shock and subsequent earthquake centroids. (b) The percentages of earthquakes that occurred within ±2° from the 117 $M_s \geq 7.0$ earthquakes that were excluded because $|\Delta\tau| < 0.01$ MPa is shown as a function of distance. The majority of earthquakes that occurred within 100 km of the main shocks were included.

distance threshold is necessary because the crustal volumes where stress has been changed can be highly irregular in shape, and the source earthquakes differ in size. The distributions of earthquakes included and excluded on this basis are shown in Figure 5; the vast majority of earthquakes with absolute value of shear stress change less than 0.01 MPa were located more than 100 km from the main shock centroids.

[15] After shear stress changes are calculated, a comparison can be made between earthquakes with shear stress increase, hence consistent with triggering, and those that

occurred despite a shear stress decrease. In Table 1 these earthquakes are tallied for each of the 117 $M_s \geq 7.0$ source events. A summation shows that of the 2166 events that followed the source earthquakes and that met the stress threshold selection criteria (0.01 MPa $\leq |\Delta\tau| \leq$ 1.0 MPa), 1327 were associated with shear stress increases, and 839 with shear stress decreases. Thus ~61% of the total number of events considered are consistent with shear stress triggering and ~39% are not; stated another way, the number of apparently triggered earthquakes exceeds the number that were apparently not triggered by a factor of ~1.6. The 1327 earthquakes consistent with triggering represent ~8% of the CMT catalog (17,402 events from 1 January 1977 until 30 September 2000).

[16] An important question is whether or not the difference between the number of earthquakes that had shear stress increase and shear stress decrease is significant. Could 61% of 2166 earthquakes occurring in the tectonically active parts of the Earth correlate with calculated shear stress increases by chance?

2.2. Tests for Significance Using Synthetic Catalogs

[17] To learn about the potential variability of stress change and seismicity following the largest earthquakes, multiple synthetic catalogs were constructed for Monte Carlo analysis that replicated key features of the CMT catalog. The question addressed is whether the apparent majority of earthquakes that correlated with shear stress increase following the largest earthquakes in the CMT catalog is significant. The null hypothesis is that the majority is a chance result and that the occurrence of earthquakes both in time and space following the largest events is unrelated to shear stress change. What is needed then is a way to assess what the variability of shear stress calculations is likely to be.

[18] Synthetic earthquake catalogs should bear as many similarities to the CMT catalog as possible to replicate natural variability, yet also must fulfill the null hypothesis. A completely random catalog in time and space would satisfy the null hypothesis, but it would fail to represent the organized behavior inherent in the CMT catalog, since earthquakes cluster along tectonic boundaries, and they cluster in time. However, a synthetic catalog that too closely resembles the actual catalog may not be sufficiently unlinked from the stress transfer hypothesis. Thus the synthetic catalogs used here have several characteristics in common with the CMT catalog, but also random features, including the following: (1) earthquake source times are kept the same as in the CMT catalog so that clusters in time are preserved (needed to meet the null-hypothesis condition that aftershocks off the main shock fault plane are unrelated to shear stress change), (2) the CMT catalog shows unequal distribution in earthquake depth, dip, and rake and random distribution of strike (Figure 6) even in small areas (Figure 7); the synthetic catalogs are drawn at random from distributions of these shapes, (3) latitudes and longitudes of individual earthquake centroids are perturbed to fall randomly within ±50 km of the original CMT locations so that the synthetic catalogs share a tendency for clustering at plate boundaries and other active zones, and (4) the b value (magnitude-frequency distribution) is the same for the CMT and synthetic catalogs.
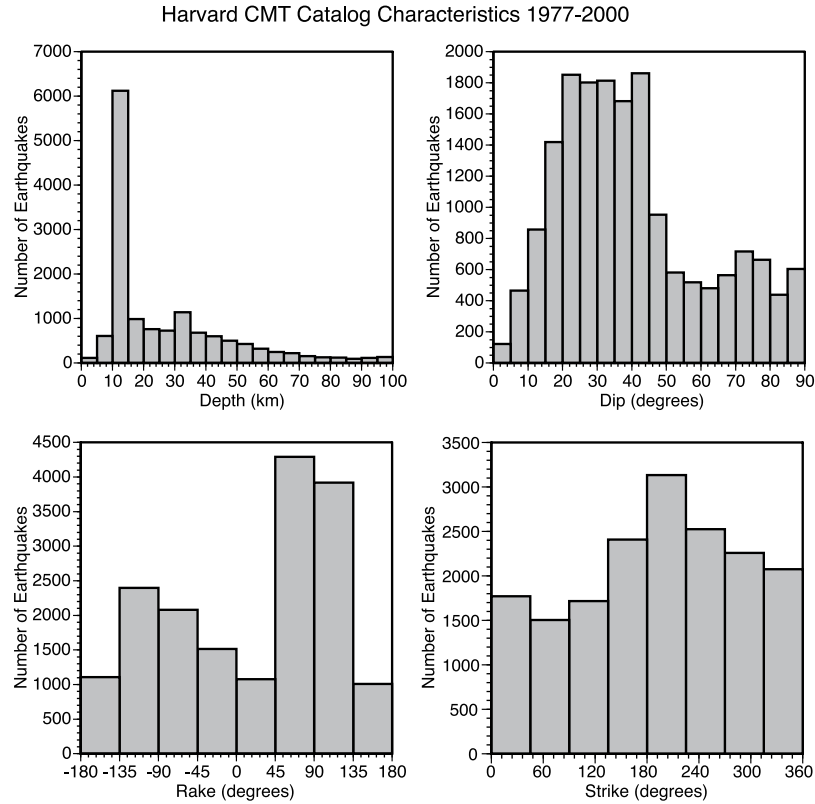
Harvard CMT Catalog Characteristics 1977-2000

Figure 6. Distributions in depth, dip, and rake, and strike of the Harvard CMT earthquake catalog. Synthetic catalogs assembled for determining the significance of the result that $\sim$61% of earthquakes following the 117 $M_s \geq 7.0$ earthquakes in the CMT catalog are associated with calculated shear stress increases are constrained to have the same distributions in depth dip and rake.

[19] The synthetic catalogs were drawn from the distributions of rake, dip, and depth of the entire CMT catalog. However, certain regions might have earthquake mechanisms that are significantly skewed from the global distribution of earthquake mechanisms. Thus the distributions of all shallow earthquakes (depth $\leq$100 km) from $4° \times 4°$ regions were compared against the overall distributions shown in Figure 6 using a Kolmogoroff-Smirnoff test, which is sensitive to differences in shapes of distributions, particularly the mean, median, dispersion, and skewness [e.g., *Sachs*, 1982]. The test statistic

$$\hat{D} = \max \left| \left(\frac{F_1}{n_1} - \frac{F_2}{n_2} \right) \right|, \tag{1}$$

where F_1 and F_2 are cumulative frequencies and n_1 and n_2 are sample sizes, is compared to the critical value

$$D_{(\alpha)} = K_{(\alpha)} \sqrt{\frac{n_1 + n_2}{n_1 n_2}}, \tag{2}$$

where $K_{(\alpha)}$ is a constant reflecting the level of significance. If $\hat{D} < D_{(\alpha)}$, then there is no demonstrable difference between the two distributions at a given confidence level. The comparisons show that, in most regions, the local distributions cannot be proven different from the whole catalog CMT distribution with 80% confidence (Figure 7).

In other words, there is no statistically significant bias toward particular focal solutions along most plate boundaries if smaller earthquakes (can include events down to $M_s = 4.5$) are included in the comparison. I thus conclude that synthetic catalogs drawn from the CMT distributions can reasonably represent local distributions.

[20] Synthetic catalogs were constructed to test the significance of the difference between the number of earthquakes that were associated with shear stress increases and decreases in the CMT catalog. Synthetic catalogs were substituted for the CMT catalog and used as described in section 2.1; shear stress changes from the 117 $M_s \geq 7.0$ real source events were calculated (rake-parallel) on synthetic receiver fault planes that fell within ±2° of the source earthquakes. Those receiver faults that showed shear stress changes ranging from ±0.01 MPa to 1 MPa were compared and tallied. After 100 such calculations, the variability of shear stress calculations resulting from different distributions of earthquakes emerges, and confidence intervals on rejecting the null hypothesis can be calculated (Figure 8). The mean ratio of shear stress increase to shear stress decrease over the 100 calculations is 50.3%, indicating that the synthetic catalogs are suitable for representing the null hypothesis. The standard deviation from the mean is 1.2%, the 95% confidence interval is 2.3%, and the null hypothesis can be rejected with 99.99% confidence at ±4.6%. The results using the real CMT catalog showed 61% of events following the largest earthquakes were associated with shear

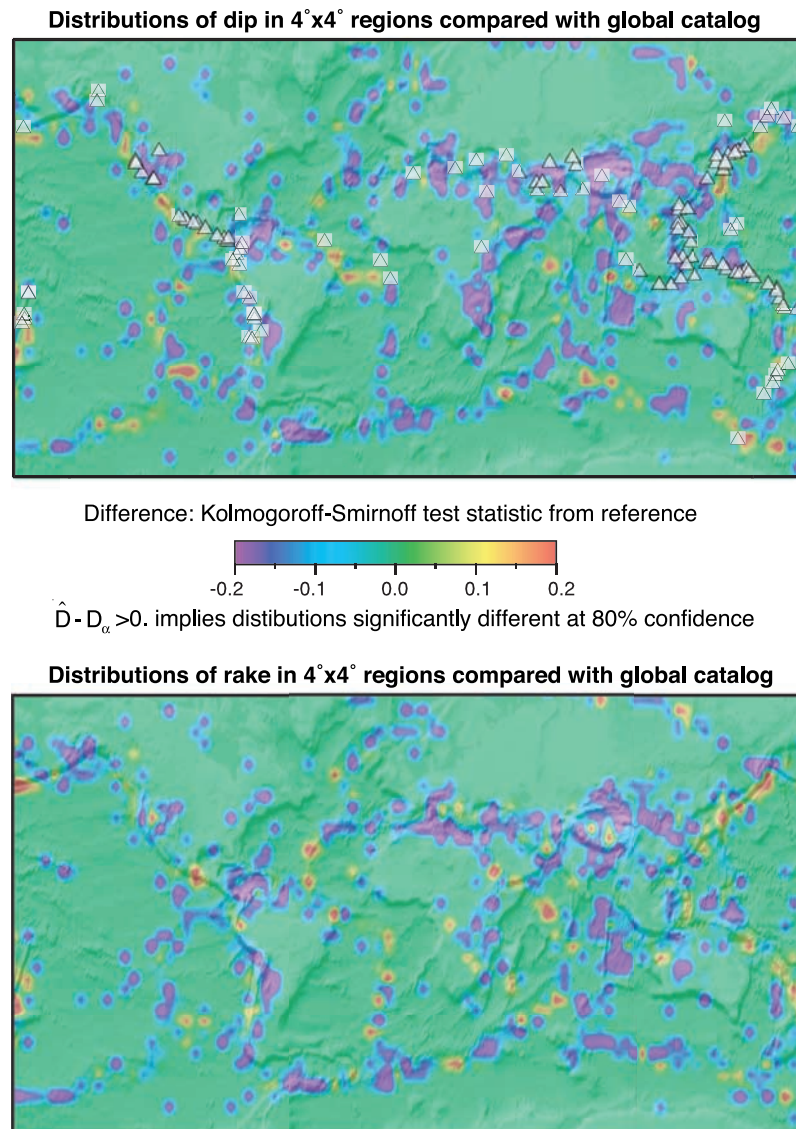**Distributions of dip in 4°x4° regions compared with global catalog**

Difference: Kolmogoroff-Smirnoff test statistic from reference

$\hat{D} - D_\alpha > 0.$ implies distibutions significantly different at 80% confidence

Distributions of rake in 4°x4° regions compared with global catalog

Figure 7. Estimate of variation in earthquake dip and rake in $4° \times 4°$ regions from global catalog distributions using a Kolmogoroff-Smirnoff test. The red-shaded areas are the only places where local distributions differ from the global distribution with 80% confidence. Triangles show the locations of the 117 $M_s \geq 7.0$ earthquakes investigated in this study as sources of triggering.

stress increase and 39% were associated with shear stress decrease; this difference of ~11% from the null-hypothesis mean of ~50% appears significant, and implies that shear stress changes caused by large earthquakes do influence the occurrence of subsequent $M_s \geq 4.5$ earthquakes.

3. Results: When and Where Are Large Triggered Aftershocks Most Likely to Occur?

[21] Calculation of shear stress changes from 117 $M_s \geq$ 7.0 earthquakes on nodal planes of subsequent earthquakes generates two populations of earthquakes, those consistent with shear stress triggering, and those that are not. The two populations are indistinguishable in terms of their b values, mean magnitudes, depths, strikes, dips, and rakes. However, differences in their rate of occurrence with time and distributions with distance from the main shock are observed.

3.1. Temporal Occurrence of Triggered Earthquakes

[22] Here the behavior of earthquakes associated with shear stress increases and decreases as a function of time is compared. If the seismicity rate of triggered earthquakes is plotted against time, it shows an Omori law decay that lasts ~7−11 years (Figure 9). Rates of earthquakes associated with calculated shear stress increases and decreases decay differently with time, as can be seen clearly in Figure 10, where the difference between the number of earthquakes that occurred before and after the main shocks is plotted as a function of time. Below I explain how the rate plots were made and discuss possible reasons for different decay rates.

3.2. Seismicity Rate Curves

[23] The curves in Figure 9 were constructed by stacking 2166 earthquakes near enough to be influenced by the

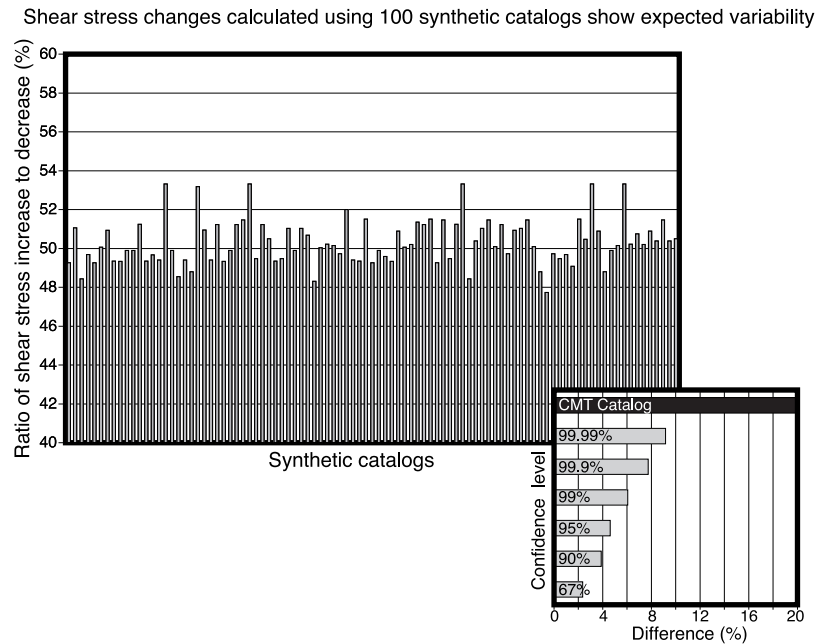Shear stress changes calculated using 100 synthetic catalogs show expected variability

Figure 8. Results of 100 calculations made with synthetic catalogs. The ratio of earthquakes from the synthetic catalogs associated with calculated shear stress increases to shear stress decreases from each calculation is shown. Confidence levels on the variation from the mean of the ratios (50.3%) are shown below and compared with the difference obtained from the real CMT catalog.

$M_s \geq 7.0$ shocks. Earthquake origin time is expressed as time elapsed since the source earthquake. Earthquakes are tallied in time bins of 1-year duration; thus the cumulative annual rate of earthquakes before and after $M_s \geq 7.0$ earthquakes is shown as a function of time relative to the source earthquakes.

[24] The background seismicity rate was established by stacking earthquakes from periods before the 117 $M_s \geq 7.0$ earthquakes (back to the beginning of the catalog) with nodal planes having calculated shear stress increases and decreases using the same threshold values as before. This was done so that the earthquake rates in the same approximate regions before and after the largest earthquakes could be compared. The background rate appears to dwindle with time away from zero in Figure 9; this is because the $M_s \geq 7.0$ earthquakes occurring later in the catalog have earthquakes associated with them for longer times than do earthquakes earlier in the catalog. For example, there are few earthquakes in the catalog near and before the great Sumba earthquake of 1977, whereas there are more than 20 years worth of events near and before the 1999 Hector Mine earthquake. The background rates are calculated separately for earthquake nodal planes associated with shear stress increases and decreases, and as might be expected, they are nearly the same (Figure 9).

[25] Just as the question was raised whether the cumulative difference between shear stress increased and decreased earthquakes is significant, it is asked whether the variation in seismicity rate versus time between the two populations is significant. In other words, since the total number of earthquakes in each time bin decreases significantly with elapsed time from the main shock, is the difference between the two populations in any given time bin greater than the natural variability? To answer this question, the same synthetic catalogs were utilized; each

time bin was examined independently, and the ratio of shear stress increased and decreased earthquakes was compared. For each bin, 100 sets of the same number of earthquakes from the same time range were gathered at random from synthetic catalogs. The ratios of earthquakes associated with calculated shear stress increases and decreases were tallied and confidence intervals were calculated (Figure 11). This process enables 95% confidence bounds to be plotted around the curves in Figure 9.

[26] The significance in the cumulative difference between the two curves was also tested using a the Kolmogoroff-Smirnoff test (see section 2.2 for full description), which evaluates two frequency distributions of different size for the likelihood that they come from the same parent distribution; the null hypothesis that the earthquake rate curves associated with calculated shear stress increases and decreases result from the same overall distribution can be rejected at the 99.9% confidence interval using the Kolmogoroff-Smirnoff test.

3.3. Spatial Occurrence of Triggered Earthquakes

[27] Earthquakes associated with calculated shear stress increases are observed at slightly different spatial distribution than those associated with shear stress decrease. Earthquakes were binned by radial distance from the source epicenter (surface projection of the centroid location), stacked, and the number occurring where shear stress was increased before the source earthquakes was subtracted from the number occurring after (Figure 12). The same process was applied to the earthquakes that were associated with calculated shear stress decreases. The difference between the two populations is not significant close to the epicenters of the source earthquakes (between 0 and 50 km) but becomes more important with increasing distance (between 50 and 250 km) (Figure 12).

Harvard CMT Catalog: Triggered Earthquake Rate vs. Time
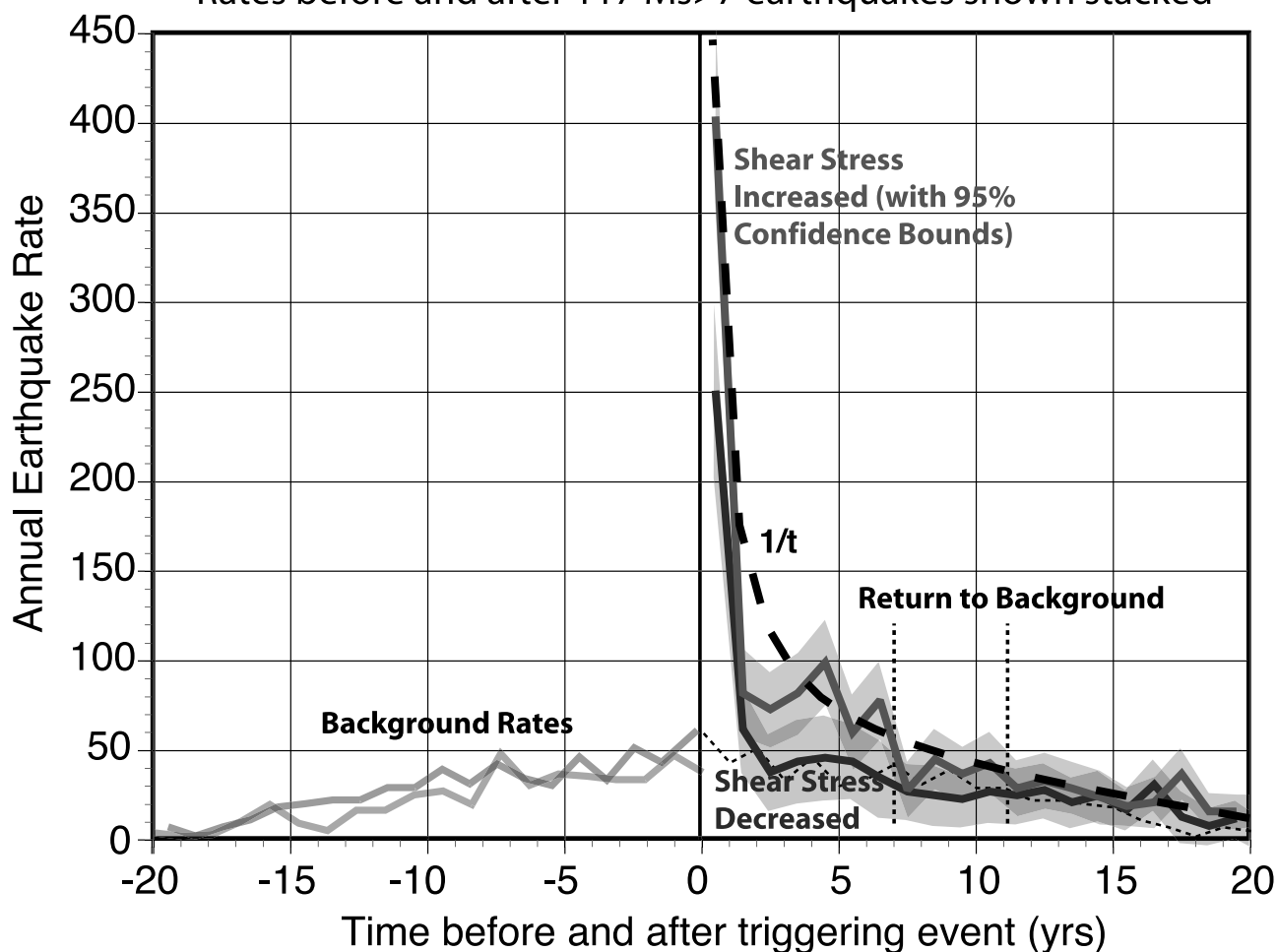### Rates before and after 117 Ms>7 earthquakes shown stacked

Figure 9. Stacked annual rate of earthquakes following the 117 $M_s \geq 7.0$ earthquakes. Upper solid gray curve shows the rate of earthquakes associated with calculated shear stress increases, and the lower solid gray line shows the rate of earthquakes associated with calculated shear stress decreases. Both sets of earthquakes show significantly higher rates immediately after the source earthquakes, but the rates of events associated with shear stress increases remains higher than background rates for ~7–11 years, whereas the rate of events associated with shear stress decreases returns to background rates within ~1–2 years. The 95% confidence bounds are plotted as shaded areas around rate curves. Background rates are calculated from the same regions of shear stress increase (solid dark line) and decrease (dashed light line) calculated from the 117 $M_s \geq 7.0$ earthquakes, but were taken from the periods before the large shocks. The seismicity rate from regions of calculated shear stress increase is reflected about the zero time axis (light dashed line) to provide a reference background rate. The rate curves approach zero at long times from the triggering earthquakes because the largest earthquakes occurring earlier in the catalog have earthquakes associated with them for longer times than do earthquakes later in the catalog.

The number of earthquakes that represent the 95% confidence bounds resulting from random variability for the total number of earthquakes in each bin is plotted in Figure 12; confidence bounds were calculated in the same manner as described in sections 2.2 and 3.1. It is assumed that the source earthquake has no influence on earthquake occurrence where differences in seismicity rate before and after shear stress changes approaches the 95% confidence intervals. There are two features of the plots shown in Figure 12 that result from the way earthquakes were selected: (1) since earthquakes were binned with radial distance from the source epicenters,

more are expected with greater distance because surface area grows proportionally to the radius squared, and (2) the stress change thresholds used (events associated with changes between ±0.01−1 MPa) to exclude earthquakes with very large and very small shear stress changes causes relatively fewer earthquakes to appear in the closest and farthest distance bins.

[28] The key difference in the locations of the earthquakes associated with shear stress increases and decreases is that earthquakes associated with calculated shear stress increases occur at distances up to 240 km from the source

Earthquakes associated with shear stress decrease
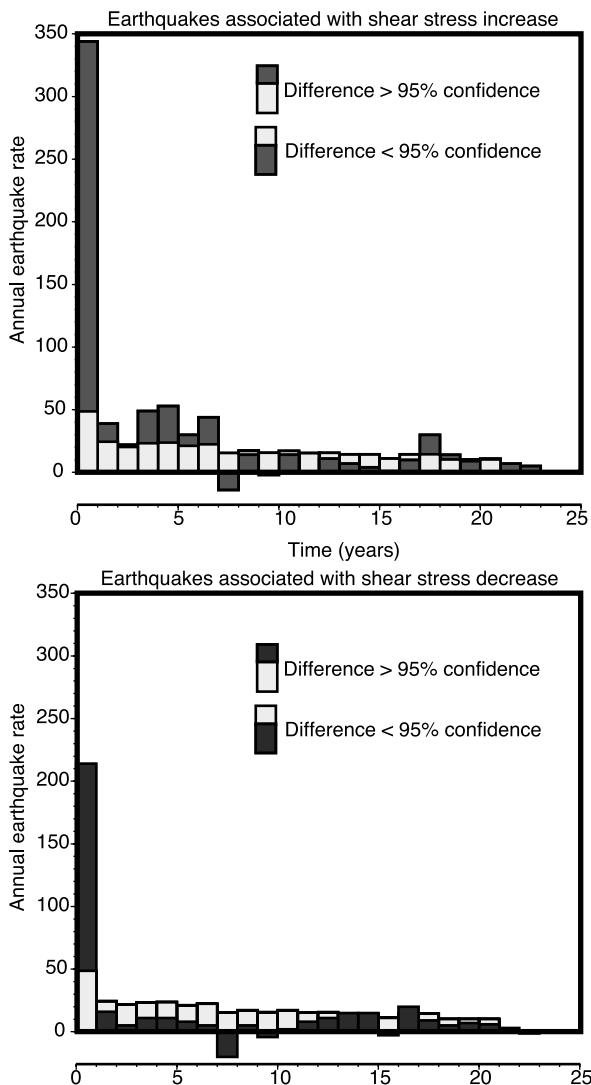return to background rate within 1 year after the mainshock

Figure 10. The difference between the number of earthquakes that occurred before the main shocks is subtracted from the number that occurred after. The earliest time that the rate is indistinguishable from background occurs when the difference is less than the 95% confidence level calculated using synthetic catalogs. This occurs at ~7 years for earthquakes associated with calculated shear stress increases and ~1 year for earthquakes associated with calculated shear stress decreases.

epicenters, while earthquakes associated with shear stress decreases are confined to distances less than about 120−140 km from the epicenters (Figure 10). Thus the bulk of the shear-stress-decreased earthquake population occurs mostly in the first 1−2 years after the source earthquake, and relatively close to the source epicenter. By comparison, the shear-stress-increased earthquake population occurs more broadly in time and space (Figures 9, 10, and 12). Application of the Kolmogoroff-Smirnoff test [e.g., *Sachs*, 1982] to the two spatial distributions shows that the possibility that they result from the same parent distribution can be rejected at the 99% confidence interval.

3.4. What Causes the Difference in Rate Versus Time and Spatial Distribution for Earthquakes Associated With Shear Stress Increases and Decreases?

[29] Earthquakes associated with calculated shear stress increases and decreases following the 117 $M_s \geq 7.0$ earthquakes show an immediate and sharp rate increase above background (Figure 9). However, there were significantly more (400 versus 250) earthquakes associated with calculated shear stress increases in the first year, and the shear-stress-increased rate persists above background for ~7−11 years while the shear-stress-decreased population returns to background rates within ~2 years (Figures 9 and 10). The tendency for earthquakes associated with calculated shear stress decreases to occur at the background rate after 1−2 years implies that these events were unrelated to the preceding earthquakes and would have happened regardless; they obviously were not suppressed by the shear stress decreases either. An interesting group of earthquakes are those that were associated with calculated shear stress decreases, yet showed a marked rate increase for the first 1−2 years following the largest earthquakes.

[30] Four explanations for the short-lived rate increase among earthquakes that were associated with calculated shear stress decreases are discussed here: normal stress change triggering, calculation errors, stress diffusion, and dynamic triggering. Since only shear stress change calculations were made in this study, earthquakes that were promoted primarily through normal stress changes would be missed. However, it is difficult to explain why the rate of earthquakes triggered by normal stress change should decay so much faster than those promoted by shear stress change. Indeed, when normal stress change calculations were made on both nodal planes of the two populations of earthquakes (first two years of earthquakes associated with shear stress increases and decreases), no observable differences could be
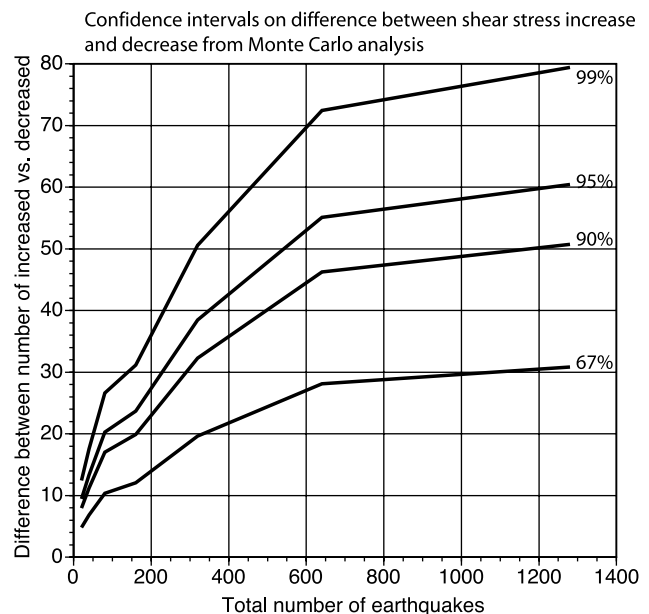

Figure 11. Confidence intervals on the difference between the number of earthquakes associated with calculated shear stress increase and decrease as a function of the number of earthquakes compared.
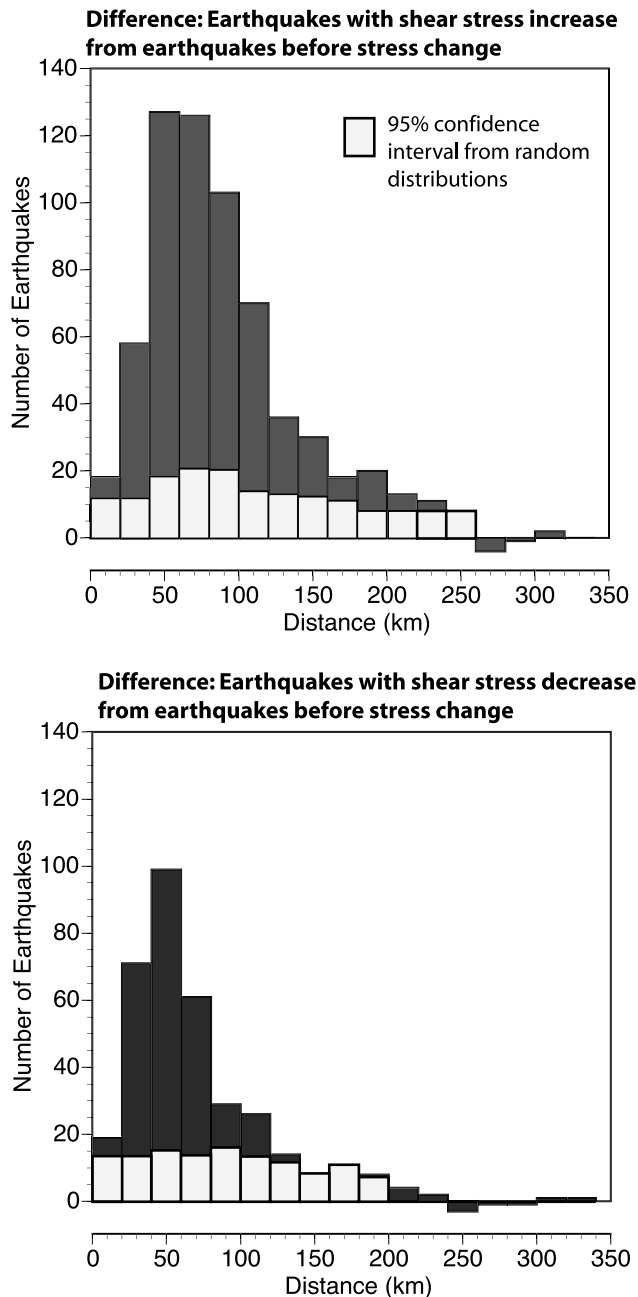
Difference: Earthquakes with shear stress increase from earthquakes before stress change

95% confidence interval from random distributions

Difference: Earthquakes with shear stress decrease from earthquakes before stress change

Figure 12. Difference between the stacked number of earthquakes associated with calculated shear stress increases before the 117 $M_s \geq 7.0$ earthquakes subtracted from the stacked number after (above) as a function of distance from the triggering earthquake centroid. The difference between earthquakes associated with calculated shear stress decreases are shown below. Earthquakes associated with shear stress increases tend to occur in greater numbers than the background at distances up to ~240 km from the triggering earthquake centroids whereas earthquakes associated with shear stress decreases occur in numbers greater than background at distances up to 140 km from the triggering centroids. 95% confidence bounds for each distance range are shown superimposed on the columns.

isolated. This observation is in accordance with studies by *Kagan* [1994] and *Kagan and Jackson* [1998], who noted no dependence on normal stress in global catalogs.

[31] Stress change calculations are sensitive to the orientations and relative locations of the earthquake rupture planes, which have been greatly simplified as single planar dislocations here. It is probable that some proportion of the earthquakes associated with shear stress decreases might be so erroneously, though a roughly equal number of those associated with shear stress increases would also be in error because there is a finite number of earthquakes in the overall population.

[32] A further complicating factor is the recognition that postearthquake deep afterslip and viscoelastic relaxation of the lower crust and upper mantle can act to redistribute stress into the seismogenic crust over time [e.g., *Nur and Mavko*, 1974; *Savage and Prescott*, 1978]. Such stress diffusion might spread rapidly with time, as has been modeled after the Landers earthquake [e.g., *Pollitz*, 2002], and might act to curtail earthquakes associated with calculated shear stress decreases and further enhance those associated with shear stress increases.

[33] Earthquakes associated with calculated shear stress increases are observed to occur at greater distances from the main shock centroids. When these spatial distribution effects are also considered, dynamic triggering may be the most plausible explanation for the differences between the shear-stress-increased and -decreased earthquake populations. For example, the Landers and Hector Mine earthquakes demonstrated directivity in dynamic triggering both near the ruptures and at great distances [e.g., *Kilb et al.*, 2000; *Gomberg et al.*, 2001]. Thus dynamic triggering, while poorly understood, is independent of the spatial patterns associated with static stress triggering and may also explain why earthquakes associated with calculated shear stress decreases that occurred above background rates did so only for a short time after the source earthquakes. Dynamic triggering might not have to occur instantaneously with the passage of seismic waves if their effect is to weaken faults slightly [e.g., *Gomberg et al.*, 1998; *Marone*, 2000]. Dynamically triggered earthquakes might also make up an important percentage of earthquakes associated with calculated static stress increases, particularly those that happen shortly after the main shock.

4. Foreshocks, Main Shocks, Aftershocks, and Rate/State Friction

[34] Of the 117 $M_s \geq 7.0$ earthquakes modeled in this study, 13 were associated with subsequent larger magnitude earthquakes that occurred within ±2°; 8 of those earthquakes (~62%) were associated with calculated shear stress increases, and 5 were associated with calculated shear stress decreases. The catalog of all 1327 subsequent earthquakes associated with calculated shear stress increases from 117 $M_s \geq 7.0$ earthquakes contains 75 earthquakes of $M_s \geq 6.5$, 23 earthquakes of $M_s \geq 7.0$, and 3 shocks with $M_s \geq 8.0$. Thus many of these apparently triggered earthquakes have magnitudes that are usually associated with the term "main shock." The earthquakes that triggered these large earthquakes could then be referred to as "foreshocks." The earthquakes associated with calculated shear stress increases

exhibit Omori law decay in rate versus time despite some of them occurring at distances up to 240 km away from the source earthquakes, and thus can be considered "aftershocks." Only semantic differences appear to separate these earthquakes, which can be unified under the concept of earthquake interaction and stress transfer. Also requiring an explanation is a global observation of Omori law decay in the rate of triggered earthquakes.

[35] Exponential decay of the rate of triggered earthquakes is a prediction made from rate and state friction theory. Laboratory experiments with simulated fault zones demonstrated that failure stress is dependent on the time of contact (state) and slip speed (rate) [e.g., *Dieterich*, 1978; *Ruina*, 1983]. The dependence is suggested to result from changes in the age and population of contact points in the fault, with older, more static contacts having greater strength than younger ones introduced by slip on the fault [*Dieterich*, 1979]. The resisting stress can thus be expressed as

$$\tau_r = (\sigma_n - p)\left[\mu_0 + A\ln\left(\frac{V}{V^*} + 1\right) + B\ln\left(\frac{\theta}{\theta^*} + 1\right)\right], \quad (3)$$

where σ_n is the normal stress, p is pore fluid pressure, μ_0, A, and B are experimentally determined constants, V^* and θ^* are normalizing constants, V is slip speed, and θ is the state variable [*Dieterich*, 1992].

[36] In rate and state friction, a stress change on a fault results in a change in slip speed, and also a transient increase or decrease in the rate of earthquakes as a consequence of slip acceleration. The resulting transient earthquake rate lasts until $V(t)$ returns to its unperturbed state. The transient earthquake rate change is predicated on the existence of multiple faults, or fault patches each with varying initial slip speeds and states, thus with varying nucleation potential (nucleation occurs when a fault patch undergoes rapidly accelerating slip). *Dieterich* [1994] derived a time-dependent seismicity rate $R(t)$, after a stress perturbation as

$$R(t) = \frac{r}{\left[\exp\left(\frac{-\Delta\tau}{A\sigma}\right) - 1\right]\exp\left[\frac{-t}{t_a}\right] + 1}, \quad (4)$$

where r is the steady state seismicity rate, $\Delta\tau$ is shear stress change, σ is the normal stress, and t_a is the observed aftershock duration, a fault-specific parameter. *Dieterich* [1994] has applied equation (4) to the global earthquake clustering statistics of *Kagan and Jackson* [1991] and to aftershocks, noting that $R(t)$ has the form of Omori's law.

[37] As discussed above, rate and state theory provides a theoretical basis for understanding earthquake clustering after a stress change; the concepts are equally applicable to on-fault aftershocks and more distant triggered earthquakes. This study shows that the majority of the earthquakes in the global CMT catalog associated with shear stress increases cluster in time, and that their rate decays exponentially. Thus the results presented here can be viewed as consistent with *Dieterich*'s [1994] predictions.

5.   Hazard Implications

[38] Global observation of triggered earthquakes indicates that their likelihood with time takes the form of

Omori's law. If prior earthquakes have influenced nearby faults, then the probability that they will fail should incorporate a transient, exponential decay with time. One means of incorporating a transient probability change with time was developed from rate and state friction theory.

5.1.   Earthquake Probability Calculations

[39] The transient change in expected earthquake rate $R(t)$ after a stress step can be related to the probability of an earthquake of a given size over the time interval Δt through a nonstationary Poisson process as

$$P(t, \Delta t) = 1 - \exp\left[-\int_t^{t+\Delta t} R(t)dt\right] = 1 - \exp[-N(t)], \quad (5)$$

after *Dieterich and Kilgore* [1996], where $N(t)$ is the expected number of earthquakes in the interval Δt. This transient probability change is added to the permanent change. Integrating equation (4) for $N(t)$ yields

$$N(t) = r_p\left\{\Delta t + t_a \ln\left[\frac{1 + \left[\exp\left(\frac{-\Delta\tau}{a\sigma}\right) - 1\right]\exp\left[\frac{-\Delta t}{t_a}\right]}{\exp\left(\frac{-\Delta\tau}{a\sigma}\right)}\right]\right\}, \quad (6)$$

where r_p is the expected rate of earthquakes associated with the permanent probability change. The rate $N(t)$ can be determined by again applying a nonstationary Poisson probability expression as

$$r_p = (-1/\Delta t)\ln(1 - P_c), \quad (7)$$

where P_c is a conditional probability, and can be calculated using any distribution [*Dieterich and Kilgore*, 1996].

[40] Rate and state transient functions have been used to calculate interaction earthquake probabilities in the Kobe, Japan, region [*Toda et al.*, 1998] and in Turkey [*Stein et al.*, 1997; *Parsons et al.*, 2000]. Results from this study confirm that globally, earthquake interactions cause marked $M_s \geq 4.5$ earthquake rate increases followed by exponential decay with time; it thus seems prudent that earthquake probability calculations incorporating stress perturbations should also include its transient effect on seismicity rate (Figure 13) as was done in the Kobe and Turkey studies.

5.2.   El Salvador 2001: Is Quick Application of Global Observations Warranted?

[41] In this study, global statistics on where and when most triggered earthquakes are expected have been compiled. Earthquake rate plots give a relative rate with time as compared with background rate; these ratios may be applied because the b value of triggered earthquakes is the same as the background. In addition to relative time plots, the expected ratio of triggered earthquakes to background can be plotted as a function of distance from the epicenter of the source earthquake. Using these plots could allow immediate assessment of expected triggered earthquake hazard following a $M_s \geq 7.0$ earthquake, and can be in place until more detailed studies are made. In this section I discuss an example application of the global results to a large earthquake that occurred in El Salvador in 2001.
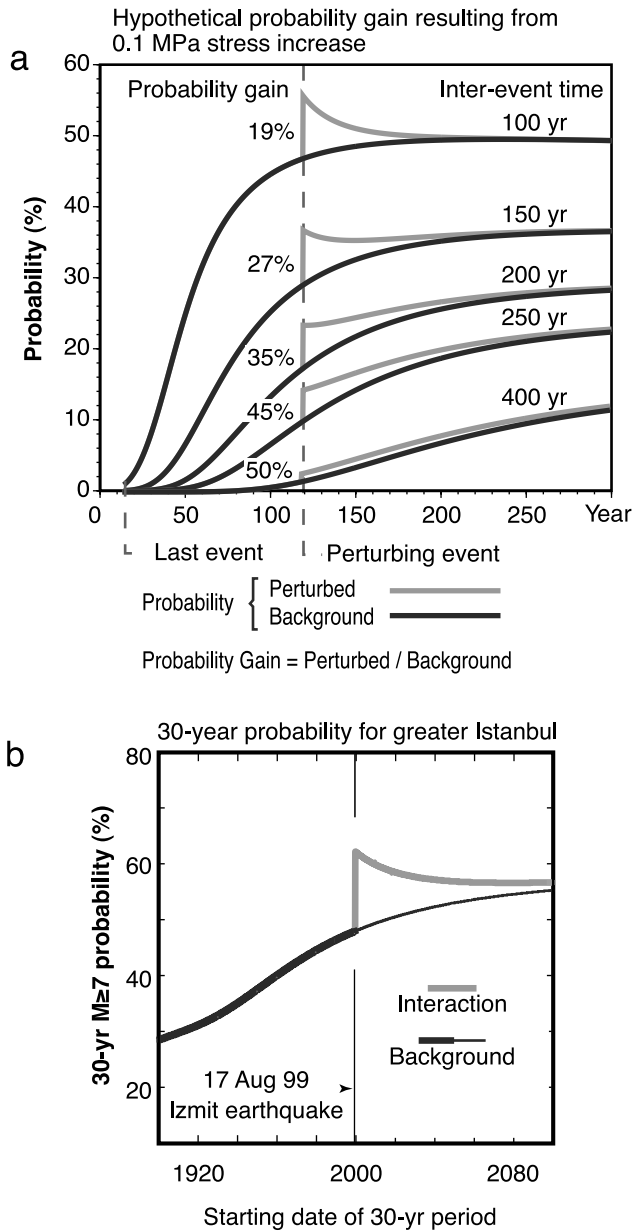
Figure 13. (a) Examples of transient earthquake probability caused by a stress increase of 0.1 MPa occurring 120 years after the last known earthquake on hypothetical faults with interevent times ranging from 100 to 400 years using equations (5)–(7). (b) A real example of earthquake probability calculated for the city of Istanbul incorporating the stress increases calculated on nearby faults from the 1999 $M = 7.4$ Izmit earthquake using a rate and state transient function [*Parsons et al.*, 2000].

Figure 14. Example of a possible application of global statistics on earthquake rate versus time and relative occurrence with distance following a $M_s \geq 7.0$ earthquake to the 13 January 2001 $M = 7.7$ El Salvador earthquake. (a) As soon as an epicenter is known, contours of most likely triggered earthquake occurrence versus distance (expressed as a ratio to background) can be plotted. In the El Salvador example, a region near the coastline is identified where twice the normal number of earthquakes of $M_s \geq 4.5$ are expected to occur over the 7–11 year period when rates are above background based on global observations. (b) The rate versus time plot below shows the relative annual rate of $M_s \geq 4.5$ earthquakes expected as a ratio of the background rate. Heavy gray curve is derived from this study, and the solid black line is t^{-1}. In the first year after the $M = 7.7$ shock, 8 times the normal rate of $M_s \geq 4.5$ earthquakes are expected. The 13 February 2001 $M = 6.6$ earthquake occurred within a zone where twice the normal number of earthquakes of $M_s \geq 4.5$ are expected and in a period when 8 times the normal rate is expected.

[42] A major earthquake occurred off the coast of El Salvador about 110 km south-southeast of San Salvador on 13 January 2001 (1133 LT in El Salvador) (Figure 14). A moment magnitude of 7.7 was computed for this earthquake. The main shock was a normal faulting event located within the subducting Cocos plate. As of 21 January 2001 the death toll was 704, with 4055 people injured and 573,609 people affected nationwide. 496 landslides were recorded; 69,714 houses were destroyed and 104,865 dam-
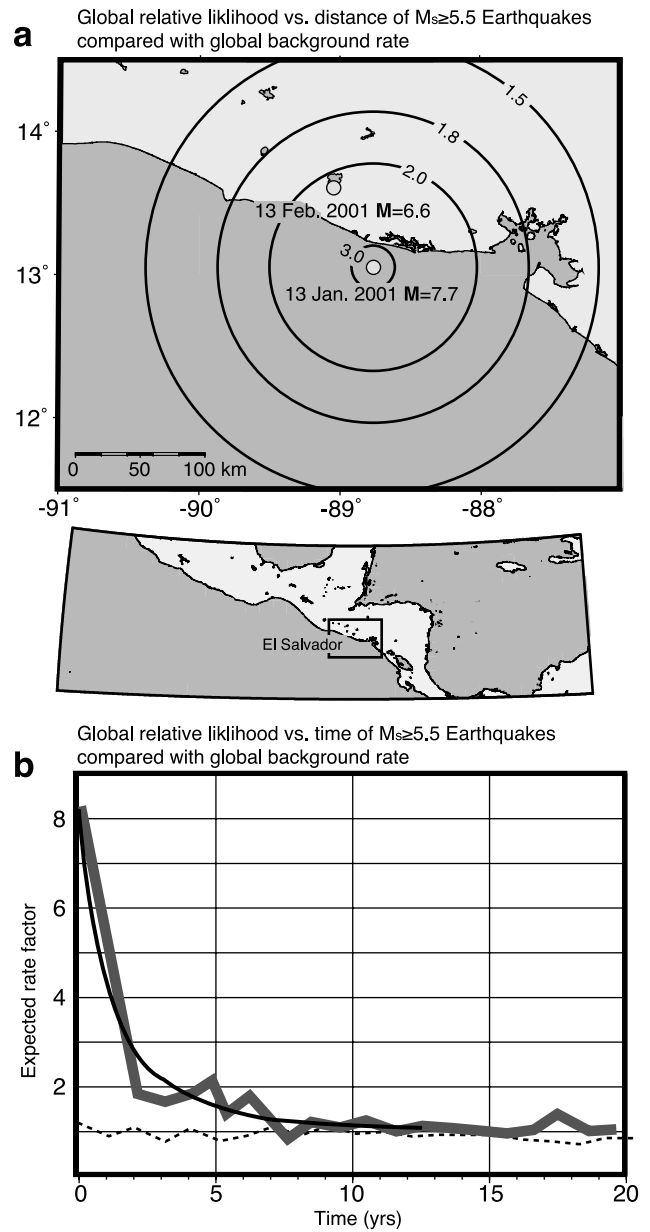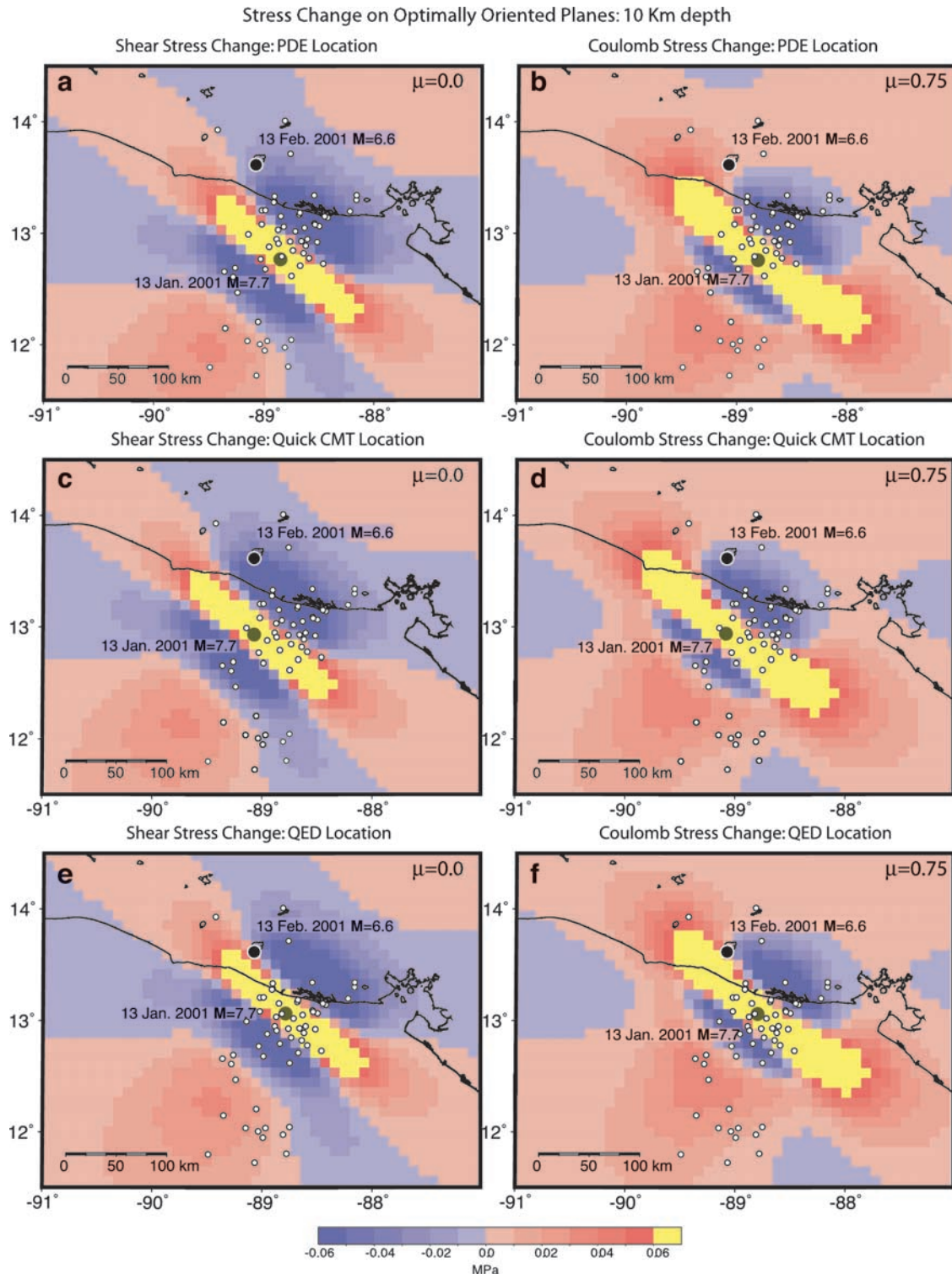
Figure 15. Coulomb stress calculations using earliest available epicentral parameters are shown along with effects of using different friction coefficients. In theory, making stress change calculations immediately after a large earthquake such as the 13 January 2001 $M = 7.7$ El Salvador shock might narrow the region where large triggered earthquakes are expected. However, as can be seen in the stress change plots, the 13 February 2001 $M = 6.6$ earthquake is located either in zones of Coulomb stress decrease or increase depending on choice of epicenter of the $M = 7.7$ earthquake, and choice of friction coefficient used in the Coulomb calculations. Once enough aftershocks (30 days of aftershock epicenters are shown as open circles) are recorded to help in the choice of friction coefficient, and earthquake source mechanisms are known, then stress change calculations may have more utility for hazard analysis.

aged by the earthquake. Some 60,000 people were moved to temporary shelters. In Figure 14a, global average relative earthquake occurrence versus distance contours are plotted from the epicenter of the El Salvador earthquake (Quick Epicentral Determination (QED) location). These contours show the likelihood of large aftershocks as a factor of the background rate versus distance from the epicenter. The coastal region nearest the epicenter would thus be expected to see twice the normal number of earthquakes for a period between ~7 and 11 years as shown by the time decay curve (Figure 14b) derived by correcting the global rate curve shown in Figure 8 for a constant background rate. In addition, the time decay curve shows that earthquakes are ~8 times more likely to happen in the first year after the source earthquake than they would 7–11 years later (Figure 14b).

[43] On 13 February 2001 (0822 LT in El Salvador), another large earthquake shook El Salvador, this time about 30 km east of San Salvador (Figure 14). A moment magnitude of 6.6 was computed for this strike-slip earthquake. The 13 February earthquake affected 221,832 people, causing 311 deaths, and 3399 injuries; it destroyed 13,935 houses and damaged 38,699 more. The 13 February earthquake was about 85 km away from the 13 January $M = 7.7$ earthquake and ~30 km shallower (Figure 14). This earthquake occurred in a region where, from global observations, about twice as many earthquakes would be expected to happen over the duration of aftershocks, and it occurred within a time range when earthquakes are expected at 8 times the normal rate.

[44] Plots from global averages may have some utility in quantifying the relative risk from triggered earthquakes. The plots from the global data are not sensitive to the mechanism and size of a particular triggering event; detailed stress-change calculation from an individual earthquake could better locate areas of heightened stress (e.g., Figures 1–3). However, Coulomb calculations require knowledge of several parameters such as a friction coefficient, coseismic pore fluid pressure change, as well as knowledge of local stress field and/or target fault orientations and rakes. If in the El Salvador example, shear or Coulomb stress is calculated on optimally oriented planes, more detailed regions of stress increase and decrease are identified; however, the results are highly dependent on friction coefficient and earthquake location (Figure 15). Variation in the earliest available locations of the 13 January $M = 7.7$ event combined with uncertainty in the friction coefficient causes stress change calculations that show the 13 February $M = 6.6$ earthquake located either in a stress shadow or a heightened stress region (Figure 15). It may thus be preferable to delay stress change calculations until better earthquake locations are available, and when more aftershocks have occurred, which can help delimit the friction coefficient [e.g., *Reasenberg and Simpson*, 1992; *Hardebeck et al.*, 1998; *Parsons et al.*, 1999].

6. Conclusions

[45] About 61% of modeled earthquakes that followed the 117 $M_s \geq 7.0$ earthquakes in the Harvard CMT catalog are associated with calculated shear stress increases, and obey an Omori law rate decay with time. It takes ~7–11 years for the rate of triggered earthquakes to return to background rates after a large earthquake. The remaining ~39% of modeled earthquakes are associated with calculated shear stress decreases and have rates higher than background for ~1–2 years and rapidly return to background rates; these earthquakes may be dynamically triggered. Earthquakes associated with calculated shear stress increases occur at higher than background rates up to 240 km from the main shocks, ~100 km farther than earthquakes associated with calculated shear stress decreases. Characteristic distributions of triggered earthquakes in space and time enable rapid determination of their likelihood after a $M_s \geq 7.0$ earthquake. Coulomb or shear stress change calculations can more accurately identify regions at risk, but fairly detailed knowledge of parameters is necessary, which may not become available until it is too late.

References

Adamek, S., F. Tajima, and D. S. Wiens, Seismic rupture associated with subduction of the Cocos ridge, *Tectonics*, 6, 757–774, 1987.

Ammon, C. J., T. Lay, A. A. Velasco, and J. E. Vidale, Routine estimation of earthquake source complexity; the 18 October 1992 Colombian earthquake, *Bull. Seismol. Soc. Am.*, 84, 1266–1271, 1994.

Astiz, L., and H. Kanamori, An earthquake doublet in Ometepec, Guerrero, Mexico, *Phys. Earth Planet. Inter.*, 34, 24–45, 1984.

Balakina, L. M., A. I. Zakharova, A. G. Moskvina, and L. S. Chepkunas, Iranian earthquake of May 10, 1997; a consistent manifestation of seismogenesis, *Phys. Solid Earth*, 36, 1–11, 2000.

Beckers, J., and T. Lay, Very broadband seismic analysis of the 1992 Flores, Indonesia, earthquake ($M_w = 7.9$), *J. Geophys. Res.*, 100, 18,179–18,193, 1995.

Beeler, N. M., R. W. Simpson, S. H. Hickman, and D. A. Lockner, Pore fluid pressure, apparent friction, and Coulomb failure, *J. Geophys. Res.*, 105, 25,533–25,542, 2000.

Berberian, M., J. A. Jackson, M. Ghorashi, and M. H. Kadjar, Field and teleseismic observations of the 1981 Golbaf-Sirch earthquakes in SE Iran, *Geophys. J. R. Astron. Soc.*, 77, 809–838, 1984.

Bezzeghoud, M., D. Dimitrov, J. C. Ruegg, and K. Lammali, Faulting mechanism of the El Asnam (Algeria) 1954 and 1980 earthquakes from modelling of vertical movements, *Tectonophysics*, 249, 249–266, 1995.

Bossu, R., and J. Grasso, Stress analysis in the intraplate area of Gazli, Uzbekistan, from different sets of earthquake focal mechanisms, *J. Geophys. Res.*, 101, 17,645–17,659, 1996.

Bullen, K. E., and B. A. Bolt, *An Introduction to the Theory of Seismology*, 499 pp., Cambridge Univ. Press, New York, 1947.

Calmant, S., B. Pelletier, R. Pillet, M. Regnier, P. Lebellegard, D. Maillard, F. Taylor, M. Bevis, and J. Recy, Interseismic and coseismic motions in GPS series related to the M_s 7.3 July 13, 1994, Malekula earthquake, central New Hebrides subduction zone, *Geophys. Res. Lett.*, 24, 3077–3080, 1997.

Campos, J., R. Madariaga, and C. Scholz, Faulting process of the August 8, 1993, Guam earthquake: A thrust event in an otherwise weakly coupled subduction zone, *J. Geophys. Res.*, 101, 17,581–17,596, 1996.

Chael, E. P., and G. S. Stewart, Recent large earthquakes along the middle America trench and their implications for the subduction process, *J. Geophys Res.*, 87, 329–338, 1982.

Chatelain, J., R. K. Cardwell, and B. L. Isaacks, Expansion of the aftershock zone following the Vanuatu (New Hebrides) earthquake on 15 July 1981, *Geophys. Res. Lett.*, 10, 385–388, 1983.

Chou, N. P., and J. H. Wang, A study on source rupture of the 1978 Lan-Hsu, southeastern Taiwan earthquake, *J. Terrest. Atmos. Oceanic Sci.*, 3, 1–20, 1992.

Cotton, F., M. Campillo, A. Deschamps, and B. K. Rastogi, Rupture history and seismotectonics of the 1991 Uttarkashi, Himalaya earthquake, *Tectonophysics*, 258, 35–51, 1996.

Dieterich, J. H., Time-dependent friction and the mechanics of stick-slip, *Pure Appl. Geophys.*, 116, 790–806, 1978.

Dieterich, J. H., Modeling of rock friction, 1, Experimental results and constitutive equations, *J. Geophys. Res.*, 84, 2161–2168, 1979.

Dieterich, J. H., Earthquake nucleation on faults with rate- and state-dependent strength, *Tectonophysics*, *211*, 115–134, 1992.

Dieterich, J. H., A constitutive law for the rate of earthquake production and its application to earthquake clustering, *J. Geophys. Res.*, *99*, 2601–2618, 1994.

Dieterich, J. H., and B. Kilgore, Implications of fault constitutive properties for earthquake prediction, *Proc. Natl. Acad. Sci. U.S.A.*, *93*, 3787–3794, 1996.

Dmowska, R., L. C. Lovison-Golob, and J. J. Durek, Partial breaking of a mature seismic gap: The 1987 earthquakes in New Britain, *Pure Appl. Geophys.*, *136*, 459–477, 1991.

Dreger, D. S., and A. Kaverina, Seismic remote sensing for earthquake source process and near-source strong shaking: A case study of the October 16, 1999 Hector Mine earthquake, *Geophys. Res. Lett.*, *27*, 1941–1944, 2000.

Duquesnoy, T., O. Bellier, M. Kasser, M. Sebrier, C. Vigny, and I. Bahar, Deformation related to the 1994 Liwa earthquake derived from geodetic measurements, *Geophys. Res. Lett.*, *23*, 3055–3058, 1996.

Dutton, C. E., *Earthquakes in the Light of the New Seismology*, 314 pp., G. P. Putnam's, New York, 1904.

Dziewonski, A. M., T.-A. Chou, and J. H. Woodhouse, Determination of earthquake source parameters from waveform data for studies of global and regional seismicity, *J. Geophys. Res.*, *86*, 2825–2852, 1981.

Eissler, H., and H. Kanamori, A large normal fault earthquake at the junction of the Tonga trench and the Louisville ridge, *Phys. Earth Planet. Inter.*, *29*, 161–172, 1982.

Ekstrom, G., and E. R. Engdahl, Earthquake source parameters and stress distribution in the Adak Island region of the central Aleutian Islands, Alaska, *J. Geophys. Res.*, *94*, 15,499–15,519, 1989.

Ellsworth, W. L., Earthquake history, 1769–1989, in The *San Andreas Fault System, California*, edited by R. E. Wallace, *U.S. Geol. Surv. Prof. Pap., 1515*, 153–187, 1990.

Estabrook, C. H., J. L. Nabelek, and A. L. Lerner-Lam, Tectonic model of the Pacific-North American plate boundary in the Gulf of Alaska from broadband analysis of the 1979 St. Elias, Alaska, earthquake and its aftershocks, *J. Geophys. Res.*, *97*, 6587–6612, 1992.

Fuenzalida, H., L. A. Rivera, H. Haessler, D. Legrand, H. Philip, L. Dorbath, D. A. McCormack, S. S. Arefiev, C. J. Langer, and A. Cisternas, Seismic source study of the Racha-Dzhava (Georgia) earthquake from aftershocks and broad-band teleseismic body-wave records; an example of active nappe tectonics, *Geophys. J. Int.*, *130*, 29–46, 1997.

Girdler, R. W., and D. A. McConnell, The 1990 to 1991 Sudan earthquake sequence and the extent of the East African rift system, *Science*, *264*, 67–70, 1994.

Gomberg, J., N. M. Beeler, M. L. Blanpied, and P. Bodin, Earthquake triggering by transient and static deformations, *J. Geophys. Res.*, *103*, 24,411–24,426, 1998.

Gomberg, J., P. A. Reasenberg, P. Bodin, and R. A. Harris, Earthquake triggering by seismic waves following the Landers and Hector Mine earthquakes, *Nature*, *411*, 462–466, 2001.

Hagerty, M. T., and S. Schwartz, The 1992 Cape Mendocino earthquake: Broadband determination of source parameters, *J. Geophys. Res.*, *101*, 16,043–16,058, 1996.

Hardebeck, J. L., J. J. Nazareth, and E. Hauksson, The static stress change triggering model: Constraints from two southern California earthquake sequences, *J. Geophys. Res.*, *103*, 24,427–24,437, 1998.

Harris, R. A., Introduction to special section: Stress triggers, stress shadows, and implications for seismic hazard, *J. Geophys. Res.*, *103*, 24,347–24,358, 1998.

Harris, R. A., and R. W. Simpson, The 1999 M_w 7.1 Hector Mine, California earthquake: A test of the stress shadow hypothesis?, *Bull. Seismol. Soc. Am.*, in press, 2002.

Hartzell, S., and C. Mendoza, Application of an iterative least-squares waveform inversion of strong-motion and teleseismic records to the 1978 Tabas, Iran earthquake, *Bull. Seismol. Soc. Am.*, *81*, 305–331, 1991.

Houston, H., and H. Kanamori, Source spectra of great earthquakes; teleseismic constraints on rupture process and strong motion, *Bull. Seismol. Soc. Am.*, *76*, 19–42, 1986.

Ihmle, P. F., and J. Ruegg, Source tomography by simulated annealing using broad-band surface waves and geodetic data; application to the M_w = 8.1 Chile 1995 event, *Geophys. J. Int.*, *131*, 146–158, 1997.

Johnson, J. M., Y. Tanioka, K. Satake, and L. J. Ruff, Two 1993 Kamchatka earthquakes, *Pure Appl. Geophys.*, *144*, 633–647, 1995.

Kagan, Y. Y., Incremental stress and earthquakes, *Geophys. J. Int.*, *117*, 345–364, 1994.

Kagan, Y. Y., and D. D. Jackson, Long-term earthquake clustering, *Geophys. J. Int.*, *104*, 117–133, 1991.

Kagan, Y. Y., and D. D. Jackson, Spatial aftershock distribution: Effect of normal stress, *J. Geophys. Res.*, *103*, 24,453–24,467, 1998.

Kanamori, H., and K. C. McNally, Variable rupture mode of the subduction zone along the Ecuador-Colombia coast, *Bull. Seismol. Soc. Am.*, *72*, 1214–1253, 1982.

Khan, S. A., T. Qaisar, and M. Mahmood, Baluchistan, Pakistan earthquake of February 27, 1997, *J. Seismol. Res.*, *22*, 316–323, 1999.

Kikuchi, M., Y. Yamanaka, K. Abe, and Y. Morita, Source rupture process of the Papua New Guinea earthquake of July 17, 1998 inferred from teleseismic body waves, *Earth Planets Space*, *51*, 1319–1324, 1999.

Kilb, D. L., J. Gomberg, and P. Bodin, Triggering of earthquake aftershocks by dynamic stresses, *Nature*, *408*, 570–574, 2000.

King, G. C. P., R. S. Stein, and J. Lin, Static stress changes and the triggering of earthquakes, *Bull. Seismol. Soc. Am.*, *84*, 935–953, 1994.

Kiratzi, A. A., and C. A. Langston, Moment tensor inversion of the 1983 January 17 Kefallinia event of Ionian Islands (Greece), *Geophys. J. Int.*, *105*, 529–535, 1991.

Kisslinger, C., and A. Hasegawa, Seismotectonics of intermediate-depth earthquakes from properties of aftershock sequences, *Tectonophysics*, *197*, 27–40, 1991.

Kreemer, C., and W. E. Holt, What caused the March 25, 1998 Antarctic Plate earthquake? Inferences from regional stress and strain rate fields, *Geophys. Res. Lett.*, *27*, 2297–2300, 2000.

Langer, C. J., and S. Hartzell, Rupture distribution of the 1977 western Argentina earthquake, *Phys. Earth Planet. Inter.*, *94*, 121–132, 1996.

Lundgren, P. R., E. A. Okal, and D. A. Wiens, Rupture characteristics of the 1982 Tonga and 1986 Kermadec earthquakes, *J. Geophys. Res.*, *94*, 15,521–15,539, 1989.

Lynnes, C. S., and T. Lay, Source processes of the great 1977 Sumba earthquake, *J. Geophys. Res.*, *93*, 13,407–13,420, 1988.

Marone, C., Shaking faults loose, *Nature*, *408*, 533–535, 2000.

Mellors, R. J., F. L. Vernon, G. L. Pavlis, G. A. Abers, M. W. Hamburger, S. Ghose, and B. Iliasov, The M_s = 7.3 1992 Suusamyr, Kyrgyzstan, earthquake, 1, Constraints on fault geometry and source parameters based on aftershocks and body-wave modeling, *Bull. Seismol. Soc. Am.*, *87*, 11–22, 1997.

Mendoza, C., Finite-fault analysis of the 1979 March 14 Petatlan, Mexico earthquake using teleseismic *P* waveforms, *Geophys. J. Int.*, *121*, 675–683, 1995.

Mendoza, C., and S. Hartzell, Fault-slip distribution of the 1995 Colima-Jalisco, Mexico, earthquake, *Bull. Seismol. Soc. Am.*, *89*, 1338–1344, 1999.

Mendoza, C., S. Hartzell, and T. Monfret, Wide-band analysis of the 3 March 1985 central Chile earthquake: Overall source process and rupture history, *Bull. Seismol. Soc. Am.*, *84*, 269–283, 1994.

Mikumo, T., Miyatake, and M. A. Santayo, Dynamic rupture of asperities and stress change during a sequence of large interplate earthquakes in the Mexican subduction zone, *Bull. Seismol. Soc. Am.*, *88*, 686–702, 1998.

Millen, D. W., and M. W. Hamburger, Seismological evidence for tearing of the Pacific Plate at the northern termination of the Tonga subduction zone, *Geology*, *26*, 659–662, 1998.

Mori, J., C. McKee, and H. Letz, The central New Britain earthquake of May 10, 1985; tensional stress in the frontal arc, *Phys. Earth Planet. Inter.*, *48*, 73–78, 1987.

Mozaffari, P., L. Xu, Z. Wu, and T. Chen, Moment tensor inversion of the November 6, 1988 M_s = 7.6, Lancang-Gengma, China, earthquake using long-period body-waves data, *Acta Seismol. Sin., Engl. Transl.*, *12*, 379–389, 1999.

Nakayama, W., and M. Takeo, Slip history of the 1994 Sanriku-Haruka-Oki, Japan, earthquake deduced from strong-motion data, *Bull. Seismol. Soc. Am.*, *87*, 918–931, 1997.

Needham, R. E., R. P. Buland, G. L. Choy, J. W. Dewey, E. R. Engdahl, S. A. Sipkin, W. Spence, and M. D. Zirbes, Special earthquake report for the September 1, 1981, Samoa Islands region earthquake, *U.S. Geol. Surv. Open File Rep., OF 82-0781*, 74 pp., 1982.

Nur, A., and G. Mavko, Postseismic viscoelastic rebound, *Science*, *183*, 204–206, 1974.

Okada, Y., Internal deformation due to shear and tensile faults in a half-space, *Bull. Seismol. Soc. Am.*, *82*, 1018–1040, 1992.

Okal, E. A., Historical seismicity and seismogenic context of the great 1979 Yapen and 1996 Biak, Irian Jaya earthquakes, *Pure Appl. Geophys.*, *154*, 633–675, 1999.

Ozel, N., and T. Moriya, Different stress directions in the aftershock focal mechanisms of the Kushiro-Oki earthquake of Jan. 15, 1993, SE Hokkaido, Japan, and horizontal rupture in the double seismic zone, *Tectonophysics*, *313*, 307–327, 1999.

Parsons, T., and D. S. Dreger, Static-stress impact of the 1992 Landers earthquake sequence on nucleation and slip at the site of the 1999 M = 7.1 Hector Mine earthquake, southern California, *Geophys. Res. Lett.*, *27*, 1949–1952, 2000.

Parsons, T., R. S. Stein, R. W. Simpson, and P. A. Reasenberg, Stress sensitivity of fault seismicity: A comparison between limited–offset ob-

lique and major strike-slip faults, *J. Geophys. Res.*, *104*, 20,183–20,202, 1999.

Parsons, T., S. Toda, R. S. Stein, A. Barka, and J. H. Dieterich, Heightened odds of large earthquakes near Istanbul: an interaction-based probability calculation, *Science*, *288*, 661–665, 2000.

Pegler, G., and S. Das, The 1987–1992 Gulf of Alaska earthquakes, *Tectonophysics*, *257*, 111–136, 1996.

Perfettini, H., R. S. Stein, R. Simpson, and M. Cocco, Stress transfer by the 1988–1989 M = 5.3 and 5.4 Lake Elsman foreshocks to the Loma Prieta fault: Unclamping at the site of peak mainshock slip, *J. Geophys. Res.*, *104*, 20,169–20,182, 1999.

Piatanesi, A., P. Heinrich, and S. Tinti, The October 4, 1994 Shikotan, Kuril Islands tsunamigenic earthquake: An open problem on the source mechanism, *Pure and Applied Geophysics*, *154*, 555–574, 1999.

Pierce, K. L., and L. A. Morgan, The track of the Yellowstone hot spot: Volcanism, faulting, and uplift, in *Regional Geology of Eastern Idaho and Western Wyoming*, edited by P. K. Link et al., *Mem. Geol. Soc. Am.*, *179*, 1–53, 1992.

Pinar, A., and N. Turkelli, Source inversion of the 1993 and 1995 Gulf of Aqaba earthquakes, *Tectonophysics*, *283*, 279–288, 1997.

Pollitz, F. F., Stress triggering of the 1999 Hector Mine earthquake by transient deformation following the 1992 Landers earthquake, *Bull. Seismol. Soc. Am.*, in press, 2002.

Protti, M., and S. Y. Schwartz, Mechanics of back arc deformation in Costa Rica; evidence from an aftershock study of the April 22, 1991, Valle de la Estrella, Costa Rica, earthquake (M_w = 7.7), *Tectonics*, *13*, 1093–1107, 1994.

Protti, M., et al., The March 25, 1990 (M_w = 7.0, M_l = 6.8), earthquake at the entrance of the Nicoya Gulf, Costa Rica: Its prior activity, foreshocks, aftershocks, and triggered seismicity, *J. Geophys. Res.*, *100*, 20,345–20,358, 1995.

Reasenberg, P. A., and R. W. Simpson, Response of regional seismicity to the static stress change produced by the Loma Prieta earthquake, *Science*, *255*, 1687–1690, 1992.

Reilinger, R. E., et al., Coseismic and postseismic fault slip for the 17 August 1999, M = 7.5, Izmit, Turkey earthquake, *Science*, *289*, 1519–1524, 2000.

Richards-Dinger, K. B., and P. M. Shearer, Earthquake locations in Southern California obtained using source-specific station terms, *J. Geophys. Res.*, *105*, 10,939–10,960, 2000.

Robinson, R. T. Amadottir, J. Beavan, J. Cousins, C. Pearson, M. Reyners, R. Van Dissen, and T. Webb, The M_w = 6.7 Arthur's Pass earthquake in the Southern Alps, New Zealand, June 18, 1994, *Seismol. Res. Lett.*, *66*, 11–13, 1995.

Rogozhin, E. A., Focal mechanism of the Neftegorsk, Sakhalin earthquake of May 27 (28), 1995, *Geotectonics*, *30*, 124–131, 1996.

Ruff, L., J. Given, and C. Sanders, The tectonics of the Macquarie Ridge, New Zealand; new evidence of strike-slip motion from the earthquake of May 25, 1981, M_w = 7.7, *Eos Trans. AGU*, *63*, 384, 1982.

Ruina, A., Slip instability and state variable friction laws, *J. Geophys. Res.*, *88*, 10,359–10,370, 1983.

Ryan, H. F., and D. W. Scholl, Geologic implications of great interplate earthquakes along the Aleutian arc, *J. Geophys. Res.*, *98*, 22,135–22,146, 1993.

Sachs, L., *Applied Statistics*, 707 pp., Springer-Verlag, New York, 1982.

Satake, K., The mechanism of the 1983 Japan Sea earthquake as inferred from long-period surface waves and tsunamis, *Phys. Earth Planet. Inter.*, *37*, 249–260, 1985.

Savage, J. C., and W. H. Prescott, Asthenospheric readjustment and the earthquake cycle, *J. Geophys. Res.*, *83*, 3369–3376, 1978.

Schwartz, S. Y., Noncharacteristic behavior and complex recurrence of large subduction zone earthquakes, *J. Geophys. Res.*, *104*, 23,111–23,125, 1999.

Simpson, R. W., and P. A. Reasenberg, Earthquake-induced static-stress changes on central California faults, *U.S. Geol. Surv. Prof. Pap.*, *1550-F*, 55–89, 1994.

Sobiesiak, M. M., Fault plane structure of the Antofagasta, Chile earthquake of 1995, *Geophys. Res. Lett.*, *27*, 577–580, 2000.

Stein, R. S., A. A. Barka, and J. H. Dieterich, Progressive failure on the North Anatolian fault since 1939 by earthquake static stress triggering, *Geophys. J. Int.*, *128*, 594–604, 1997.

Swenson, J. L., and S. L. Beck, Source characteristics of the 12 November 1996 M_w 7.7 Peru subduction earthquake, *Pure Appl. Geophys.*, *154*, 731–751, 1999.

Tanioka, Y., and F. Gonzalez, The Aleutian earthquake of June 10, 1996 (M_w 7.9) ruptured parts of both the Andreanof and Delarof segments, *Geophys. Res. Lett.*, *25*, 2245–2248, 1998.

Tanioka, Y., and V. Hsu, Source parameters of the April 18 and 19, 1990 Minahasa Peninsula earthquakes, *Eos Trans. AGU*, *71*, 1438, 1990.

Tanioka, Y., and K. Satake, Tsunami generation by horizontal displacement of ocean bottom, *Geophys. Res. Lett.*, *23*, 861–864, 1996.

Toda, S., R. S. Stein, P. A. Reasenberg, J. H. Dieterich, and A. Yoshida, Stress transferred by the 1995 M_w = 6.9 Kobe, Japan, shock: Effect on aftershocks and future earthquake probabilities, *J. Geophys. Res.*, *103*, 24,543–24,565, 1998.

Uidas, A., *Principles of Seismology*, 475 pp., Cambridge Univ. Press, New York, 1999.

Utsu, T., Statistical study on the occurrence of aftershocks, *Geophys. Mag.*, *30*, 521–605, 1961.

Van Dissen, R., J. Cousins, R. Robinson, and M. Reyners, The Fiordland earthquake of 10 August, 1993; a reconnaissance report covering tectonic setting, peak ground acceleration, and landslide damage, *Inst. Geol. Nucl. Sci. Contrib.*, *230*, 147–154, 1994.

Velasco, A. A., C. J. Ammon, and T. Lay, Source time function complexity of the great 1989 Macquarie ridge earthquake, *J. Geophys. Res.*, *100*, 3989–4009, 1995.

Velasco, A. A., C. J. Ammon, T. Lay, and M. Hagerty, Rupture process of the 1990 Luzon, Philippines (M_w = 7.7), earthquake, *J. Geophys. Res.*, *101*, 22,419–22,434, 1996.

Vidale, J., and H. Kanamori, The October 1980 earthquake sequence near the New Hebrides, *Geophys. Res. Lett.*, *10*, 1137–1140, 1983.

Wald, D. J., Rupture model of the 1989 Loma Prieta earthquake from the inversion of strong-motion and broadband teleseismic data, *Bull. Seismol. Soc. Am.*, *81*, 1540–1572, 1991.

Wald, D. J., Slip history of the 1995 Kobe, Japan, earthquake determined from strong motion, teleseismic, and geodetic data, *J. Phys. Earth*, *44*, 489–503, 1996.

Wald, D. J., and T. H. Heaton, Spatial and temporal distribution of slip for the 1992 Landers, California earthquake, *Bull. Seismol. Soc. Am.*, *84*, 668–691, 1994.

Webb, T. H., and M. A. Lowry, The Puysegur Bank earthquake of 1979 October 12, *N. Z. J. Geol. Geophys.*, *25*, 383–395, 1982.

Wells, D. L., and K. J. Coppersmith, New empirical relationships among magnitude, rupture length, rupture width, rupture area, and surface displacement, *Bull. Seismol. Soc. Am.*, *84*, 974–1002, 1994.

Wha, S. S., The 1997 Kamchatka earthquake, *Individual Stud.*, vol. 34, pp. 91–99, Int. Inst. of Seismol. and Earthquake Eng., Tsukuba, Japan, 1998.

Xu, L., and Y. Chen, Tempo-spatial rupture process of the 1997 Mani, Xizang (Tibet), China earthquake of M_s = 7.9, *Acta Seismol. Sin.*, *12*, 495–506, 1999.

Yepes, H., The M_w 6.8 Macas earthquake in the sub-Andean zone of Ecuador, October 3, 1995, *Seismol. Res. Lett.*, *67*, 27–32, 1996.

Yoshida, Y., K. Satake, and K. Abe, The large normal-faulting Mariana earthquake of April 5, 1990 in uncoupled subduction zone, *Geophys. Res. Lett.*, *19*, 297–300, 1992.

Zhang, J., Inversion of surface wave spectra for source parameters of large earthquakes using aspherical Earth models, *Phys. Earth Planet. Inter.*, *107*, 327–350, 1998.

Zheng, T., Z. Yao, and P. Liu, The 14 November 1986 Taiwan earthquake-An event with isotropic component, *Phys. Earth Planet. Inter.*, *91*, 285–298, 1995.

Zobin, V. M., Earthquake focal mechanisms and seismotectonic deformation in the Kamchatka-Commander region, *J. Geodyn.*, *12*, 1–19, 1990.

―――――――――――

T. Parsons, U.S. Geological Survey, MS-999, 345 Middlefield Rd., Menlo Park, CA 94025, USA. (tparsons@usgs.gov)